Discontinuous Galerkin approximation of the bidomain system for cardiac electrophysiology

Numerical Analysis for Partial Differential Equations

Authors:
Marta Lorenzo
Perego Matilde

Supervisors:
Antonietti Paola Francesca
Vergara Christian

February 16, 2021

Contents

1 Introduction

The mathematical and numerical modelling of the electrophysiology of the heart has captured more and more interest between the scientific community. Due to this fact different models and numerical approaches have been proposed to deal with the problem of cardiac electrophysiology.
The two most used macroscopic models are the monodomain and the bidomain problems: two systems of partial differential equations, modelled in [1]. The principal difference among them is that the second one distinguishes between the intra-cellular and the extra-cellular conductivities, while the first one makes an hypothesis of proportionality between the two.
In order to close these systems an ODE system modeling ionic currents is needed. We opted for the *FitzHugh Nagumo* model [7], which approximates the ionic current by means of a cubic function, but other choices could be made such as the *Rogers McCulloch model* (1994) [17], and the *Bueno-Orovio* model (2008) [18]. All of these models describe the ionic current without distinguish between the different ions and compose the *reduced ionic current models* family. Two other families exist: the *first generation*, e.g. *Beeler-Reuter* (1977) [8], and *second generation*, e.g. *Luo-Rudy dynamic* model (1994) [9]. These models are more sophisticated and while the first one allows explicit description of the kinetics of different ionic currents, exploiting different gating variables, the second one introduce the description of the ion concentration.
Moreover also different choices concerning the equation of the system are possible: both a *parabolic-parabolic* (PP) and a *parabolic-elliptic* (PE) formulation have been proposed (for more details see [1]).

Concerning the numerical approximation FEM (Finite Element Method) or SEM (Semi Explicit Method) have already been used, e.g. Niederer, Kerfoot, Benson, Bernabeu, Bernus (2011) [10] or by Hüsnü Dal , Serdar Göktepe, Michael Kaliske Ellen Kuhl (2011) [11] or Ellen Kuhl and Serdar Göktepe [12]. Now we want to exploit discontinuous Galerkin (DG) methods due to the simple applicability to complex geometries, the higher order discretizations and the great degree of flexibility of the solution at the interface.

Summing up, we opted for a *parabolic-parabolic* bidomain system closed with the Fitzhugh Nagumo model for the ion current, implemented through discontinuous Galerkin method.

The aim of our project is to implement a numerical model for the bidomain problem of cardiac electrophysiology using the Discontinuous Galerkin approximation. We started from the monodomain problem implemented by two colleagues for the project of the course of Numerical Analysis of Partial Differential Equation [3].
In the first section of this work we will give a brief introduction regarding cardiac electrophysiology, followed by the presentation of the weak and algebraic formulation of the system and by its temporal discretization. Finally we will test our model and present our results.

2 Cardiac electrophysiology

Cardiac functioning is governed by the propagation of an electrical signal that causes the cells of the myocardium to contract.
At the microscopic level, this phenomenon is due to ions exchanges favored by the opening of ion channels that allow the passage of the relative substances (Na^+, K^+, Ca^-, ...).
Instead, at the macroscopic scales, the travelling of the action potential from cell to cell is allowed by the presence of the gap junctions. The single membrane cell can be modelled as a capacitor separating charges that accumulate at its intracellular and extracellular surfaces. Cells are modeled as a capacitor and a series of resistances, one for each ionic current. In the intracellular region, two adjacent cells are connected by a resistance representing a gap junction. However, the latter is not explicitly modelled at the macroscopic scales: instead its effect is hidden in the conductivity tensor. (For more details see [1])

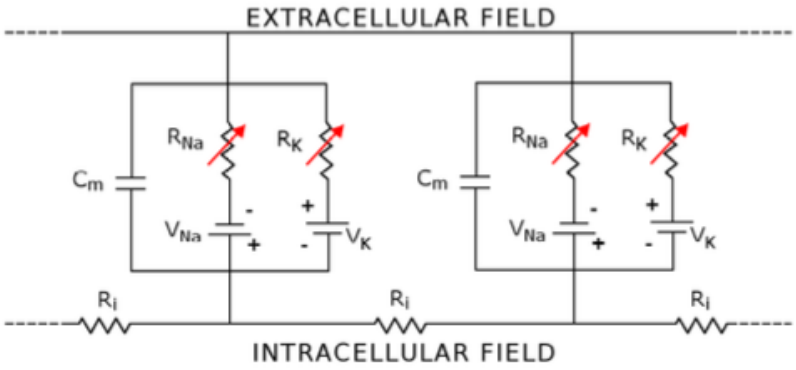

Figure 1: Electrical circuit for the sequence of two cardiac cells.

The propagation of the potentials is described by means of partial differential equations, suitably coupled with ordinary differential equations modelling the ionic currents in the cells.

3 The bidomain model

3.1 Mathematical model

We used a mathematical model consisting of two parabolic PDEs called *parabolic-parabolic* (P-P) formulation of the bidomain equations. Let $\Omega_{mus} \subset \mathbb{R}^3$ be the region occupied by the myocardium, the bidomain model reads as:

$$\begin{cases} \chi_m C_m \dfrac{\partial V_m}{\partial t} - \nabla \cdot (\Sigma_i \nabla \phi_i) + \chi_m I_{ion} = I_i^{ext} & in \quad \Omega_{mus} \times (0,T] \\ -\chi_m C_m \dfrac{\partial V_m}{\partial t} - \nabla \cdot (\Sigma_e \nabla \phi_e) - \chi_m I_{ion} = -I_e^{ext} & in \quad \Omega_{mus} \times (0,T] \end{cases}$$

where:

- χ_m is the surface to volume ratio;
- C_m is the the cellular membrane capacitance;
- Σ_i is the intracellular conductivity tensor;
- Σ_e is the extracellular conductivity tensor;
- $\phi_i(t, \boldsymbol{x})$ is the intracellular potential;
- $\phi_e(t, \boldsymbol{x})$ is the extracellular potential;
- $V_m(t, \boldsymbol{x}) = \phi_i(t, \boldsymbol{x}) - \phi_e(t, \boldsymbol{x})$ is the transmembrane potential;
- $I^i_{ext}(t, \boldsymbol{x})$ and $I^e_{ext}(t, \boldsymbol{x})$ are the intracellular and extracellular applied currents per unit volume;
- $I_{ion} = I_{ion}(V_m, \omega)$ is the ionic current, a linear function of V_m;
- ω is the gating variable, which represents the percentage of open channels per unit area of the membrane and so it represents the refractoriness of cells.

In order to describe the I_{ion}, we chose the *FitzHugh-Nagumo* model [7] i.e.:

$$\begin{cases} \mathrm{I}_{ion}(V_m, \omega) = -kV_m(V_m - a)(V_m - 1) - \omega \\ g(V_m, \omega) = \dfrac{\partial \omega}{\partial t} = \epsilon(V_m - \gamma\omega) \end{cases}$$

with k, a, γ, ϵ suitably chosen parameters.

Other choices for ionic current model are possible, such as the piecewise linear models of *Rinzel and Keller* model (1973) [14], defined as:

$$I_{ion}(V_m, \omega) = H(V_m - a) - V_m - \omega$$

where H is the Heaviside function, or the *McKean* model (1970) [13]:

$$I_{ion}(V_m, \omega) = \begin{cases} \text{- V}_m & \text{for} \quad V_m < \frac{a}{2} \\ \text{V}_m - a & \text{for} \quad \frac{a}{2} < V_m < \frac{1+a}{2} \\ \text{1 - V}_m & \text{for} \quad V_m > \frac{1+a}{2} \end{cases}$$

However the solution that we expect is the propagation of a steep front of the transmembrane potential, which is a function with very high gradients, that are difficult to grasp. So DG methods are particularly suitable for this cardiac problem, thanks to their flexibility with both mesh design and polynomial degree of freedom.

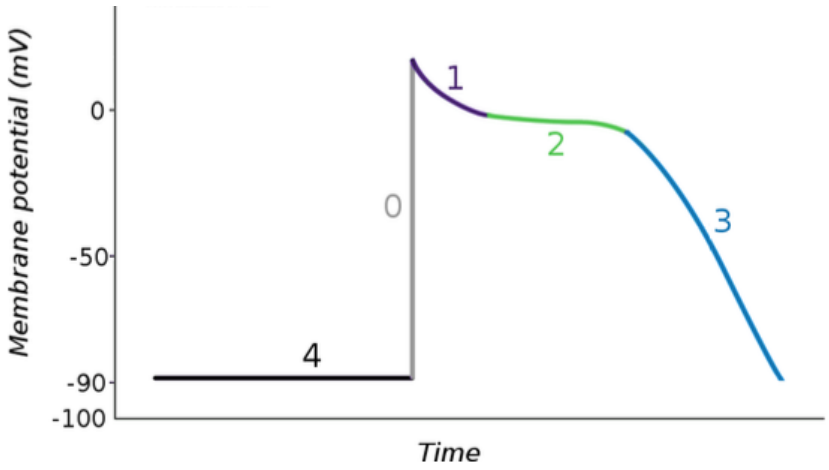

Figure 2: Propagation of action potential with realistic values

3.2 DG semi-discrete formulation

The bidomain problem reads as:

$$\begin{cases} \chi_m C_m \dfrac{\partial V_m}{\partial t} - \nabla \cdot (\Sigma_i \nabla \phi_i) + \chi_m I_{ion} = I_i^{ext} & \text{in} \quad \Omega_{mus} \times (0,T] \\ -\chi_m C_m \dfrac{\partial V_m}{\partial t} - \nabla \cdot (\Sigma_e \nabla \phi_e) - \chi_m I_{ion} = -I_e^{ext} & \text{in} \quad \Omega_{mus} \times (0,T] \\ \Sigma_i \nabla \phi_i \cdot \mathbf{n} = b_i & \text{on} \quad \partial\Omega_{mus} \times (0,T] \\ \Sigma_e \nabla \phi_e \cdot \mathbf{n} = b_e & \text{on} \quad \partial\Omega_{mus} \times (0,T] \\ \dfrac{\partial \boldsymbol{\omega}}{\partial t} = \mathbf{g}(V_m, \boldsymbol{\omega}) = \epsilon(V_m - \gamma \boldsymbol{\omega}) & \text{in} \quad \Omega_{\text{mus}} \times (0,T] \end{cases} \tag{1}$$

where b_i and b_e represent respectively the intracellular and the extracellular potential fluxes of the Neumann boundary condition functions. We introduce now a triangulation $\mathcal{T}_h$ over Ω and, for every $\mathcal{K}$ of $\mathcal{T}_h$, we multiply the parabolic equations for an elementwise smooth test function v, and then integrate over $\mathcal{K}$. We get:

$$\begin{aligned} \int_{\mathcal{K}} \chi_m C_m \frac{\partial V_m}{\partial t} v d\omega - \int_{\mathcal{K}} \nabla \cdot (\Sigma_i \nabla \phi_i) v d\omega - \int_{\mathcal{K}} \chi_m k (V_m - 1)(V_m - a) V_m v d\omega \quad + \\ - \int_{\mathcal{K}} \chi_m \boldsymbol{\omega} v = \int_{\mathcal{K}} I_i^{ext} v d\omega, \\ - \int_{\mathcal{K}} \chi_m C_m \frac{\partial V_m}{\partial t} v d\omega - \int_{\mathcal{K}} \nabla \cdot (\Sigma_e \nabla \phi_e) v d\omega + \int_{\mathcal{K}} \chi_m k (V_m - 1)(V_m - a) V_m v d\omega \quad + \\ + \int_{\mathcal{K}} \chi_m \boldsymbol{\omega} v d\omega = - \int_{\mathcal{K}} I_e^{ext} v d\omega. \end{aligned}$$

Now we have to sum all these terms for all the $\mathcal{K}$ of the triangulation.
The diffusion terms, the second terms of the left hand sides, are integrated by parts:

$$\begin{aligned} \sum_{\mathcal{K} \in \mathcal{T}_h} \int_{\mathcal{K}} \nabla \cdot (\Sigma_i \nabla \phi_i) v d\omega = \sum_{\mathcal{K} \in \mathcal{T}_h} \int_{\mathcal{K}} (\Sigma_i \nabla \phi_i) \cdot \nabla v d\omega - \sum_{\mathcal{K} \in \mathcal{T}_h} \int_{\partial \mathcal{K}} (\Sigma_i \nabla \phi_i) \cdot \mathbf{n} v d\sigma, \\ \sum_{\mathcal{K} \in \mathcal{T}_h} \int_{\mathcal{K}} \nabla \cdot (\Sigma_e \nabla \phi_e) v d\omega = \sum_{\mathcal{K} \in \mathcal{T}_h} \int_{\mathcal{K}} (\Sigma_e \nabla \phi_e) \cdot \nabla v d\omega - \sum_{\mathcal{K} \in \mathcal{T}_h} \int_{\partial \mathcal{K}} (\Sigma_e \nabla \phi_e) \cdot \mathbf{n} v d\sigma. \end{aligned}$$

where $\mathbf{n}$ is the outgoing normal vector of $\mathcal{K}$.

Let exploit the magic formula [6] to manipulate these terms:

$$\sum_{\mathcal{K} \in \mathcal{T}_h} \int_{\partial \mathcal{K}} \tau \cdot \mathbf{n}_{\mathcal{K}} v d\sigma = \sum_{F \in \mathcal{F}_h} \int_F \{\!\{\tau\}\!\} \cdot [\![v]\!] d\sigma + \sum_{F \in \mathcal{F}_h^I} \int_F [\![\tau]\!] \cdot \{\!\{v\}\!\} d\sigma \tag{2}$$

where $\mathcal{F}_h^I$ is the set of all the edges shared by two neighbouring triangles of $\mathcal{T}_h$, $\mathcal{F}_h^B$ is the set of boundary faces of $\mathcal{T}_h$ and $\mathcal{F}_h$ is the union i.e. $\mathcal{F}_h = \mathcal{F}_h^I \cup \mathcal{F}_h^B$.

We obtain:

$$\begin{aligned}
\sum_{\mathcal{K}\in\mathcal{T}_h}\int_{\mathcal{K}} \nabla\cdot(\Sigma_i\nabla\phi_i)v d\omega = \sum_{\mathcal{K}\in\mathcal{T}_h}\int_{\mathcal{K}}(\Sigma_i\nabla\phi_i)\cdot\nabla v d\omega - \sum_{F\in\mathcal{F}_h}\int_F \{\!\{\Sigma_i\nabla\phi_i\}\!\}\cdot[\![v]\!]d\sigma + \\
- \sum_{F\in\mathcal{F}_h^I}\int_F [\![\Sigma_i\nabla\phi_i]\!]\cdot\{\!\{v\}\!\}d\sigma, \\
\sum_{\mathcal{K}\in\mathcal{T}_h}\int_{\mathcal{K}} \nabla\cdot(\Sigma_e\nabla\phi_e)v d\omega = \sum_{\mathcal{K}\in\mathcal{T}_h}\int_{\mathcal{K}}(\Sigma_e\nabla\phi_e)\cdot\nabla v d\omega - \sum_{F\in\mathcal{F}_h}\int_F \{\!\{\Sigma_e\nabla\phi_e\}\!\}\cdot[\![v]\!]d\sigma + \\
- \sum_{F\in\mathcal{F}_h^I}\int_F [\![\Sigma_e\nabla\phi_e]\!]\cdot\{\!\{v\}\!\}d\sigma.
\end{aligned}$$

We notice that the last term of both equations is null due to the fact that $[\![\Sigma_i\nabla\phi_i]\!] = \mathbf{0}$ and $[\![\Sigma_e\nabla\phi_e]\!] = \mathbf{0}$.

Moreover since we require that the solutions $\mathbf{\Phi} = [\phi_i, \phi_e] \in [H^2(\Omega)]^2$ we have that $[\![\phi_i]\!] = [\![\phi_e]\!] = 0$ on all the internal faces and we can add two consistent terms to both equations:

$$\begin{aligned}
\sum_{\mathcal{K}\in\mathcal{T}_h}\int_{\mathcal{K}} \nabla\cdot(\Sigma_i\nabla\phi_i)v d\omega = \sum_{\mathcal{K}\in\mathcal{T}_h}\int_{\mathcal{K}}(\Sigma_i\nabla\phi_i)\cdot\nabla v d\omega - \sum_{F\in\mathcal{F}_h}\int_F \{\!\{\Sigma_i\nabla\phi_i\}\!\}\cdot[\![v]\!]d\sigma + \\
-\delta\sum_{F\in\mathcal{F}_h^I}\int_F \{\!\{\Sigma_i\nabla_h v\}\!\}\cdot[\![\phi_i]\!]d\sigma + \sum_{F\in\mathcal{F}_h^I}\int_F \gamma[\![\phi_i]\!]\cdot[\![v]\!]d\sigma, \\
\sum_{\mathcal{K}\in\mathcal{T}_h}\int_{\mathcal{K}} \nabla\cdot(\Sigma_e\nabla\phi_e)v d\omega = \sum_{\mathcal{K}\in\mathcal{T}_h}\int_{\mathcal{K}}(\Sigma_e\nabla\phi_e)\cdot\nabla v d\omega - \sum_{F\in\mathcal{F}_h}\int_F \{\!\{\Sigma_e\nabla\phi_e\}\!\}\cdot[\![v]\!]d\sigma + \\
-\delta\sum_{F\in\mathcal{F}_h^I}\int_F \{\!\{\Sigma_e\nabla_h v\}\!\}\cdot[\![\phi_e]\!]d\sigma + \sum_{F\in\mathcal{F}_h^I}\int_F \gamma[\![\phi_e]\!]\cdot[\![v]\!]d\sigma.
\end{aligned}$$

where δ represents the penalty constant and $\gamma \in L^\infty(\mathcal{F}_h)$ is the stabilization function, defined as: $\gamma|_{\mathcal{F}} = \alpha\dfrac{\tilde{k}^2}{\tilde{h}}$ with $\alpha \in \mathbb{R}, \alpha > 0$, $\tilde{k} = \max(k_+, k_-)$ and $\tilde{h} = \max(h_{k_+}, h_{k_-})$, where k_+, k_- are the degrees of the polynomial of the neighbouring elements, while h_{k_+}, h_{k_-} are the characteristic length of those elements.

In order to impose the Neumann boundary conditions we can analyze the second terms in the rhs of these last expressions. If we split that summations into the internal and the external faces of the triangulation, we found the boundary term that allow us to impose the boundary conditions and bring those terms on the right hand side:

$$\sum_{F\in\mathcal{F}_h}\int_F \{\!\{\Sigma_i\nabla\phi_i\}\!\}\cdot[\![v]\!]d\sigma = \sum_{F\in\mathcal{F}_h^B}\int_F \{\!\{\Sigma_i\nabla\phi_i\}\!\}\cdot[\![v]\!]d\sigma + \sum_{F\in\mathcal{F}_h^I}\int_F \{\!\{\Sigma_i\nabla\phi_i\}\!\}\cdot[\![v]\!]d\sigma =$$

$$= \sum_{F\in\mathcal{F}_h^B}\int_F \Sigma_i\nabla\phi_i\cdot\mathbf{n}v d\sigma + \sum_{F\in\mathcal{F}_h^I}\int_F \{\!\{\Sigma_i\nabla\phi_i\}\!\}\cdot[\![v]\!]d\sigma = \int_{\partial\Omega} b_i v d\sigma + \sum_{F\in\mathcal{F}_h^I}\int_F \{\!\{\Sigma_i\nabla\phi_i\}\!\}\cdot[\![v]\!]d\sigma$$

$$\sum_{F\in\mathcal{F}_h}\int_F \{\!\{\Sigma_e\nabla\phi_e\}\!\}\cdot[\![v]\!]d\sigma = \sum_{F\in\mathcal{F}_h^B}\int_F \{\!\{\Sigma_e\nabla\phi_e\}\!\}\cdot[\![v]\!]d\sigma + \sum_{F\in\mathcal{F}_h^I}\int_F \{\!\{\Sigma_e\nabla\phi_e\}\!\}\cdot[\![v]\!]d\sigma =$$

$$= \sum_{F\in\mathcal{F}_h^B}\int_F \Sigma_e\nabla\phi_e\cdot\mathbf{n}v d\sigma + \sum_{F\in\mathcal{F}_h^I}\int_F \{\!\{\Sigma_e\nabla\phi_e\}\!\}\cdot[\![v]\!]d\sigma = \int_{\partial\Omega} b_e v d\sigma + \sum_{F\in\mathcal{F}_h^I}\int_F \{\!\{\Sigma_e\nabla\phi_e\}\!\}\cdot[\![v]\!]d\sigma$$

We define the DG space $V_h^k = \{v_h \in L^2(\Omega) : v_h|_{\mathcal{K}} \in \mathbb{P}^k(\mathcal{K})\ \forall \mathcal{K}\in\mathcal{T}_h\}$ (where k is the degree of the piecewise continuous polynomial).

We now have to deal with the ODE for the gating variable ω. We multiply for a test function v_h and integrate over the triangulation $\mathcal{T}_h$ and obtain:

$$\sum_{\mathcal{K}\in\mathcal{T}_h}\int_{\mathcal{K}}\frac{\partial w_h}{\partial t}v_h d\sigma = \sum_{\mathcal{K}\in\mathcal{T}_h}\int_{\mathcal{K}}\epsilon\big(V_{m,h}-\gamma w_h\big)v_h d\sigma \qquad \forall\ v_h\in V_h^p \tag{3}$$

where $V_m^h = \phi_i^h - \phi_e^h$.

Finally we reorganize all the terms, obtaining the **semi discrete DG formulation** that reads as:

For any time $t\in[0,T]$ find $\mathbf{\Phi_h}(t) = [\phi_i^h(t), \phi_e^h(t)]^T \in [V_h^k]^2$ and $\omega_h(t)\in V_h^k$:

$$\sum_{\mathcal{K}\in\mathcal{T}_h}\int_{\mathcal{K}}\chi_m C_m\frac{\partial V_m^h}{\partial t}v_h d\omega + a_i(\phi_i^h, v_h) - \sum_{\mathcal{K}\in\mathcal{T}_h}\int_{\mathcal{K}}\chi_m k(V_m^h-1)(V_m^h-a)V_m^h v_h d\omega \quad + \\ - \sum_{\mathcal{K}\in\mathcal{T}_h}\int_{\mathcal{K}}\chi_m w_h v_h d\omega = (I_i^{ext}, v_h) \qquad \forall\ v_h\in V_h^p$$

$$-\sum_{\mathcal{K}\in\mathcal{T}_h}\int_{\mathcal{K}}\chi_m C_m\frac{\partial V_m^h}{\partial t}v_h d\omega + a_e(\phi_e^h, v_h) + \sum_{\mathcal{K}\in\mathcal{T}_h}\int_{\mathcal{K}}\chi_m k(V_m^h-1)(V_m^h-a)V_m^h v_h d\omega \quad + \\ + \sum_{\mathcal{K}\in\mathcal{T}_h}\int_{\mathcal{K}}\chi_m w_h v_h d\omega = (-I_e^{ext}, v_h) \qquad \forall\ v_h\in V_h^p$$

$$\sum_{\mathcal{K}\in\mathcal{T}_h}\int_{\mathcal{K}}\frac{\partial w_h}{\partial t}v_h d\omega = \sum_{\mathcal{K}\in\mathcal{T}_h}\int_{\mathcal{K}}\epsilon(V_m^h-\gamma w_h)v_h d\omega \qquad \forall\ v_h\in V_h^p$$

where:

$$a_i(\phi_i^h,v_h)=\sum_{\mathcal{K}\in\mathcal{T}_h}\int_{\mathcal{K}}(\Sigma_i\nabla_h\phi_i^h)\cdot\nabla_h v_h d\omega-\sum_{F\in\mathcal{F}_h^I}\int_F\{\!\{\Sigma_i\nabla_h\phi_i^h\}\!\}\cdot[\![v_h]\!]d\sigma+$$
$$-\delta\sum_{F\in\mathcal{F}_h^I}\int_F\{\!\{\Sigma_i\nabla_h v_h\}\!\}\cdot[\![\phi_i^h]\!]d\sigma+\sum_{F\in\mathcal{F}_h^I}\int_F\gamma[\![\phi_i^h]\!]\cdot[\![v_h]\!]d\sigma \quad (4)$$

$$a_e(\phi_e^h,v_h)=\sum_{\mathcal{K}\in\mathcal{T}_h}\int_{\mathcal{K}}(\Sigma_e\nabla_h\phi_e^h)\cdot\nabla_h v_h d\omega-\sum_{F\in\mathcal{F}_h^I}\int_F\{\!\{\Sigma_e\nabla_h\phi_e^h\}\!\}[\![v_h]\!]d\sigma+$$
$$-\delta\sum_{F\in\mathcal{F}_h^I}\int_F\{\!\{\Sigma_e\nabla_h v_h\}\!\}\cdot[\![\phi_e^h]\!]d\sigma+\sum_{F\in\mathcal{F}_h^I}\int_F\gamma[\![\phi_e^h]\!]\cdot[\![v_h]\!]d\sigma \quad (5)$$

and

$$(I_i^{ext},v_h)=\sum_{\mathcal{K}\in\mathcal{T}_h}\int_{\mathcal{K}}I_i^{ext}v_h d\omega+\int_{\partial\Omega}bv_h d\sigma. \quad (6)$$

$$(-I_e^{ext},v_h)=-\sum_{\mathcal{K}\in\mathcal{T}_h}\int_{\mathcal{K}}I_e^{ext}v_h d\omega+\int_{\partial\Omega}bv_h d\sigma. \quad (7)$$

Moreover, according to the choice of the coefficient δ we can recover:

- $\delta=1$: SIP i.e. Symmetric Interior Penalty (Wheeler '78, Arnold '82 [15]);
- $\delta=0$: IIP i.e. Incomplete Interior Penalty (Wheeler '99 [16]);
- $\delta=-1$: NIP i.e. Non-symmetric Interior Penalty (Wheeler '99 [16]) .

3.3 Algebraic formulation

In order to obtain the algebraic formulation we introduce a basis $\{\varphi_j\}_{j=1:N_h}$, of V_h^k, so that we can test the equations with respect to the basis:

$$\mathbf{\Phi}_h(t) = \begin{bmatrix} \phi_i^h(t) \\ \phi_e^h(t) \end{bmatrix} = \begin{bmatrix} \sum_{j=1}^{N_h} \phi_{i,j}(t)\varphi_j \\ \sum_{j=1}^{N_h} \phi_{e,j}(t)\varphi_j \end{bmatrix}$$

and in particular

$$V_m^h(t) = \sum_{j=1}^{N_h} V_{m,j}(t)\varphi_j = \sum_{j=1}^{N_h} (\phi_{i,j}(t) - \phi_{e,j}(t))\varphi_j$$

We introduce now the matrices:

$$M_{kj} = \sum_{\mathcal{K}\in\mathcal{T}_h} \int_{\mathcal{K}} \varphi_j \varphi_k d\omega \qquad \text{Mass matrix} \tag{8}$$

$$A_i = V - I_i^T - \theta I_i + S \qquad \text{Intra-cellular stiffness matrix} \tag{9}$$

$$A_e = V - I_e^T - \theta I_e + S \qquad \text{Extra-cellular stiffness matrix} \tag{10}$$

where:

$$V_{kj} = \int_\Omega \nabla_h \varphi_j \cdot \nabla_h \varphi_k d\omega$$

$$S_{kj} = \sum_{F\in\mathcal{F}_h^I} \int_F \gamma \, [\![\varphi_j]\!] \cdot [\![\varphi_k]\!] d\sigma$$

$$I_{i,kj} = \sum_{F\in\mathcal{F}_h^I} \int_F [\![\varphi_j]\!] \cdot \{\!\{\Sigma_i \nabla_h \varphi_k\}\!\} d\sigma \qquad I_{i,kj}^T = \sum_{F\in\mathcal{F}_h^I} \int_F \{\!\{\Sigma_i \nabla_h \varphi_j\}\!\} \cdot [\![\varphi_k]\!] d\sigma$$

$$I_{e,kj} = \sum_{F\in\mathcal{F}_h^I} \int_F [\![\varphi_j]\!] \cdot \{\!\{\Sigma_e \nabla_h \varphi_k\}\!\} d\sigma \qquad I_{e,kj}^T = \sum_{F\in\mathcal{F}_h^I} \int_F \{\!\{\Sigma_e \nabla_h \varphi_j\}\!\} \cdot [\![\varphi_k]\!] d\sigma$$

$$C(u_h)_{kj} = -\sum_{\mathcal{K}\in\mathcal{T}_h} \int_{\mathcal{K}} \chi_m k (V_m^h - 1)(V_m^h - a)\varphi_j \varphi_k d\omega \qquad \text{Non linear matrix} \tag{11}$$

$$\boldsymbol{F_h} = \begin{bmatrix} \boldsymbol{F_i^h} \\ \boldsymbol{F_e^h} \end{bmatrix} = \begin{bmatrix} \int_\Omega I_i^{ext}\varphi_k d\omega - \sum_{F\in\mathcal{F}_h^B}\int_F b_i\varphi_k d\sigma \\ -\int_\Omega I_e^{ext}\varphi_k d\omega - \sum_{F\in\mathcal{F}_h^B}\int_F b_e\varphi_k d\sigma \end{bmatrix}$$

Define now:

$$\boldsymbol{\Phi_h} = \begin{bmatrix} \boldsymbol{\phi_i^h}(t) \\ \boldsymbol{\phi_e^h}(t) \end{bmatrix} = \begin{bmatrix} [\phi_{i,1}(t), \phi_{i,2}(t), \phi_{i,3}(t), ..., \phi_{i,N_h}(t)]^T \\ [\phi_{e,1}(t), \phi_{e,2}(t), \phi_{e,3}(t), ..., \phi_{e,N_h}(t)]^T \end{bmatrix}$$

Moreover we introduce: $w_h(t) = \sum_{j=1}^{N_h} w_j(t)\varphi_j$ and let $\boldsymbol{\omega_h} = [\omega_1(t), \omega_2(t), ..., \omega_{N_h}(t)]^T$.

Finally our algebraic formulation is:

$$\chi_m C_m M\dot{\mathbf{V}}_\mathbf{m}^\mathbf{h} + A_i\phi_\mathbf{i}^\mathbf{h} + C(\mathbf{V}_\mathbf{m}^\mathbf{h})\mathbf{V}_\mathbf{m}^\mathbf{h} - \chi_m M\boldsymbol{\omega_h} = \mathbf{F}_\mathbf{i}^\mathbf{h}$$

$$-\chi_m C_m M\dot{\mathbf{V}}_\mathbf{m}^\mathbf{h} + A_e\phi_\mathbf{e}^\mathbf{h} - C(\mathbf{V}_\mathbf{m}^\mathbf{h})\mathbf{V}_\mathbf{m}^\mathbf{h} + \chi_m M\boldsymbol{\omega_h} = \mathbf{F}_\mathbf{e}^\mathbf{h}$$

Working with a block matrix we obtain the final **algebraic formulation**:

Find a solution $\boldsymbol{\Phi_h} = [\phi_i^h(t), \phi_e^h(t)]^T \in [V_h^p]^2$ and $\omega_h \in V_h^p$ for every $t \in (0; T]$ such that:

$$\chi_m C_m \begin{bmatrix} M & -M \\ -M & M \end{bmatrix} \cdot \begin{bmatrix} \dot{\boldsymbol{\phi}}_\boldsymbol{i}^\boldsymbol{h}(t) \\ \dot{\boldsymbol{\phi}}_\boldsymbol{e}^\boldsymbol{h}(t) \end{bmatrix} + \begin{bmatrix} A_i & 0 \\ 0 & A_e \end{bmatrix} \cdot \begin{bmatrix} \boldsymbol{\phi_i^h}(t) \\ \boldsymbol{\phi_e^h}(t) \end{bmatrix} + \begin{bmatrix} C(V_m^h) & -C(V_m^h) \\ -C(V_m^h) & C(V_m^h) \end{bmatrix} \cdot \begin{bmatrix} \boldsymbol{\phi_i^h}(t) \\ \boldsymbol{\phi_e^h}(t) \end{bmatrix} +$$

$$- \chi_m \begin{bmatrix} M & 0 \\ 0 & -M \end{bmatrix} \cdot \begin{bmatrix} \boldsymbol{\omega_h}(t) \\ \boldsymbol{\omega_h}(t) \end{bmatrix} = \begin{bmatrix} \boldsymbol{F_i^h} \\ \boldsymbol{F_e^h} \end{bmatrix}$$

$$M\dot{\boldsymbol{\omega}}_\boldsymbol{h}(t) = \varepsilon M(\boldsymbol{V_m^h}(t) - \gamma\boldsymbol{\omega_h}(t))$$

4 Temporal discretization

In order to deal with the time variable we divide the interval (0,T] into K subinterval $(t^k, t^{k+1}]$ of length $\Delta t = t^{k+1} - t^k$ where $t^k = k\Delta t \qquad \forall k = 0, ..., K-1$.
For the sake of simplicity we chose to avoid writing the spatial subscript h, from this moment on.
We opt for an implicit method for the time discretization, while we chose a semi-implicit method for the non linear contribution of I^{ion}. According to the *FitzHugh Nagumo* model [7] the ionic current is a cubic function and we linearized it by evaluating the quadratic term at the previous step, while we maintained the contribution of the gating variable implicit:

$$I_{ion} = -k(\boldsymbol{V_m^k} - a)(\boldsymbol{V_m^k} - 1)\boldsymbol{V_m^{k+1}} - \boldsymbol{\omega}^{k+1}$$

Moreover since we first compute the ODE for $\boldsymbol{\omega}$ we are able to exploit an implicit contribution of this term in the monolitic system.

$$M\frac{\boldsymbol{\omega}^{k+1} - \boldsymbol{\omega}^k}{\Delta t} = \varepsilon M(\boldsymbol{V_m^k} - \gamma\boldsymbol{\omega}^{k+1})$$

Therefore we obtain:

$$\chi_m C_m \begin{bmatrix} M & -M \\ -M & M \end{bmatrix} \cdot \begin{bmatrix} \frac{\boldsymbol{\phi_i^{k+1}} - \boldsymbol{\phi_i^k}}{\Delta t} \\ \frac{\boldsymbol{\phi_e^{k+1}} - \boldsymbol{\phi_e^k}}{\Delta t} \end{bmatrix} + \begin{bmatrix} A_i & 0 \\ 0 & A_e \end{bmatrix} \cdot \begin{bmatrix} \boldsymbol{\phi_i^{k+1}} \\ \boldsymbol{\phi_e^{k+1}} \end{bmatrix} +$$

$$+ \begin{bmatrix} C(V_m^k) & -C(V_m^k) \\ -C(V_m^k) & C(V_m^k) \end{bmatrix} \cdot \begin{bmatrix} \boldsymbol{\phi_i^{k+1}} \\ \boldsymbol{\phi_e^{k+1}} \end{bmatrix} - \chi_m \begin{bmatrix} M & 0 \\ 0 & -M \end{bmatrix} \cdot \begin{bmatrix} \boldsymbol{\omega}^{k+1} \\ \boldsymbol{\omega}^{k+1} \end{bmatrix} = \begin{bmatrix} \boldsymbol{F_i^{k+1}} \\ \boldsymbol{F_e^{k+1}} \end{bmatrix}$$

where $\boldsymbol{V_m^k} = \boldsymbol{\phi_i^k} - \boldsymbol{\phi_e^k}$.

The final system to solve $\forall k = 0, ..., K-1$ is:

$$\begin{cases} \left(\frac{1}{\Delta t} + \varepsilon\gamma\right) M\boldsymbol{\omega}^{k+1} = \varepsilon M\boldsymbol{V_m^k} + \frac{M}{\Delta t}\boldsymbol{\omega}^k \\ \\ (B + C_{nl}(\boldsymbol{\phi}^k))\boldsymbol{\phi}^{k+1} = \boldsymbol{r}^{k+1} \end{cases} \tag{12}$$

where

- $B = \frac{\chi_m C_m}{\Delta t} \begin{bmatrix} M & -M \\ -M & M \end{bmatrix} + \begin{bmatrix} A_i & 0 \\ 0 & A_e \end{bmatrix}$

- $\mathrm{C}_{nl}(\boldsymbol{\phi}^k) = \begin{bmatrix} C(V_m^k) & -C(V_m^k) \\ -C(V_m^k) & C(V_m^k) \end{bmatrix}$ (with $C(\boldsymbol{V_m^k}) = -k\chi_m(\boldsymbol{V_m^k} - a)(\boldsymbol{V_m^k} - 1)$)

- $\boldsymbol{r}^{k+1} = \begin{bmatrix} \boldsymbol{F_i^{k+1}} \\ \boldsymbol{F_e^{k+1}} \end{bmatrix} + \chi_m \begin{bmatrix} M & 0 \\ 0 & -M \end{bmatrix} \cdot \begin{bmatrix} \omega^{k+1} \\ \omega^{k+1} \end{bmatrix} + \frac{\chi_m C_m}{\Delta t} \begin{bmatrix} M & -M \\ -M & M \end{bmatrix} \cdot \begin{bmatrix} \boldsymbol{\phi_i^k} \\ \boldsymbol{\phi_e^k} \end{bmatrix}$

5 A numerical example with analytical solution

The next step is to build an exact analytical solution that would satisfy the model. After that we perform the comparison through convergence test with the solution obtained numerically.

The model we use is the one previously explained, for which we chose the following methods:

- implicit method for the diffusive term
- semi-implicit for the non linear part where, in order to linearize it, we have treated explicitly a quadratic term;

We need to write two exact solutions: one for ϕ_i (intracellular potential) and another for ϕ_e (extracellular potential). We chose:

$$\tilde{\phi_i} = 2\sin(2\pi x)\sin(2\pi y)e^{-5t}$$
$$\tilde{\phi_e} = \sin(2\pi x)\sin(2\pi y)e^{-5t}$$

obtaining the following equivalence: $\tilde{V_m} = \tilde{\phi_i} - \tilde{\phi_e} = \sin(2\pi x)\sin(2\pi y)e^{-5t}$

We impose the following Neumann boundary conditions:

$$\Sigma_i \nabla\tilde{\phi_i} \cdot \boldsymbol{n} = \begin{cases} 2\Sigma_i(-2\pi\sin(2\pi x)\cos(2\pi y)e^{-5t}) & (y=0) \\ 2\Sigma_i(2\pi\cos(2\pi x)\sin(2\pi y)e^{-5t}) & (x=1) \\ 2\Sigma_i(2\pi\sin(2\pi x)\cos(2\pi y)e^{-5t}) & (y=1) \\ 2\Sigma_i(-2\pi\cos(2\pi x)\sin(2\pi y)e^{-5t}) & (x=0) \end{cases}$$

$$\Sigma_e \nabla\tilde{\phi_e} \cdot \boldsymbol{n} = \begin{cases} \Sigma_e(-2\pi\sin(2\pi x)\cos(2\pi y)e^{-5t}) & (y=0) \\ \Sigma_e(2\pi\cos(2\pi x)\sin(2\pi y)e^{-5t}) & (x=1) \\ \Sigma_e(2\pi\sin(2\pi x)\cos(2\pi y)e^{-5t}) & (y=1) \\ \Sigma_e(-2\pi\cos(2\pi x)\sin(2\pi y)e^{-5t}) & (x=0) \end{cases}$$

In particular we notice that for this boundary conditions, if we take $\Sigma_i = \Sigma_e = 1$, we obtain the same condition imposed in the monodomain problem with $\Sigma = 1$:

$$\Sigma_i \nabla \tilde{\phi}_i \cdot \boldsymbol{n} - \Sigma_e \nabla \tilde{\phi}_e \cdot \boldsymbol{n} = \nabla(2\tilde{V}_m) \cdot \boldsymbol{n} - \nabla \tilde{V}_m \cdot \boldsymbol{n} = \nabla \tilde{V}_m \cdot \boldsymbol{n} = \Sigma \nabla \tilde{V}_m \cdot \boldsymbol{n}$$

(for more details see [2]).

The applied current is analytically calculated by inserting the exact solutions in the bidomain system:

$$\begin{aligned} I_i^{ext} &= \left[-5\chi_m C_m + 16\pi^2 \Sigma_i - \chi_m k(\tilde{V}_m - 1)(\tilde{V}_m - a)\right]\tilde{V}_m - \chi_m \omega \\ -I_e^{ext} &= \left[5\chi_m C_m + 8\pi^2 \Sigma_e + \chi_m k(\tilde{V}_m - 1)(\tilde{V}_m - a)\right]\tilde{V}_m + \chi_m \omega \end{aligned}$$

where:

$$\omega = \frac{\epsilon}{\epsilon\gamma - 5}\tilde{V}_m$$

We chose unitary parameter for the PDEs:

- $\chi_m = 1$;
- $C_m = 1$;
- $\Sigma_i = 1$;
- $\Sigma_e = 1$;

and physiological parameters for the gating variable ODE:

- $k = 19.5$;
- $\varepsilon = 1.2$;
- $\gamma = 0.1$;
- $a = 0.013$.

6 A numerical example with physiological coefficients

We now report the plot of the solutions and the errors of the example we introduced in the former chapter. (We will discuss these results in section 8).

6.1 *Test case 1*

Test1: k = P1, nRef = 3, $T = 0.001$, $\Delta t = 0.0001$

Error type	**Value**
Error L^2	0.0587
Error semi-H^1	1.3895
Error H^1	1.3907
Error inf	0.0811
Error DG	1.5418

Table 1: Errors of solution V_m of ***Test 1***

Plot of V_m - transmembrane potential:

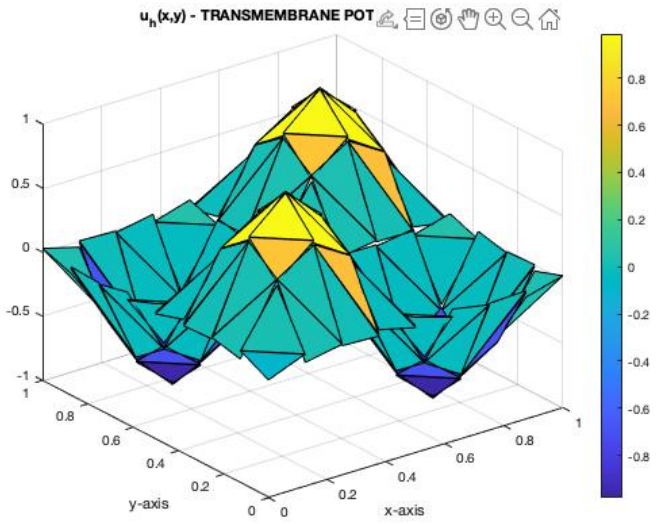

Figure 3: Numerical solution of V_m

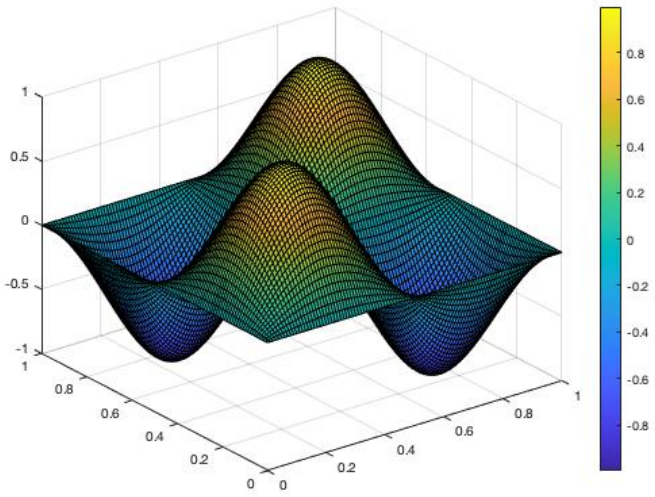

Figure 4: Analytical solution of V_m

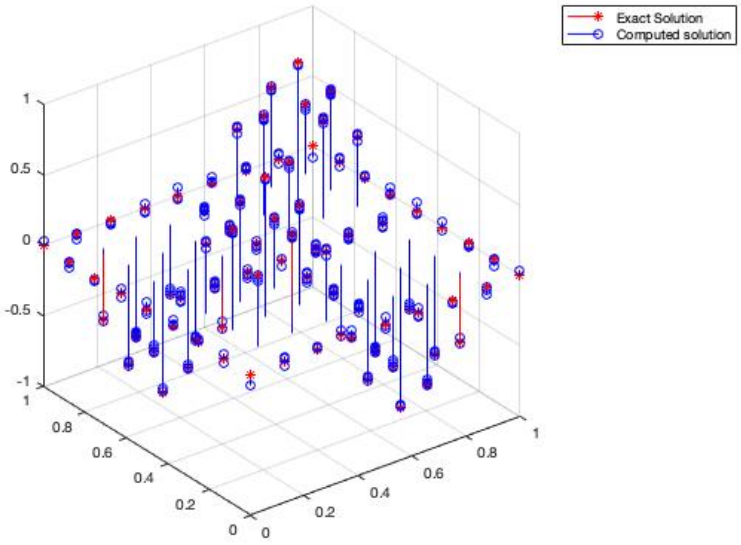

Figure 5: Error of V_m

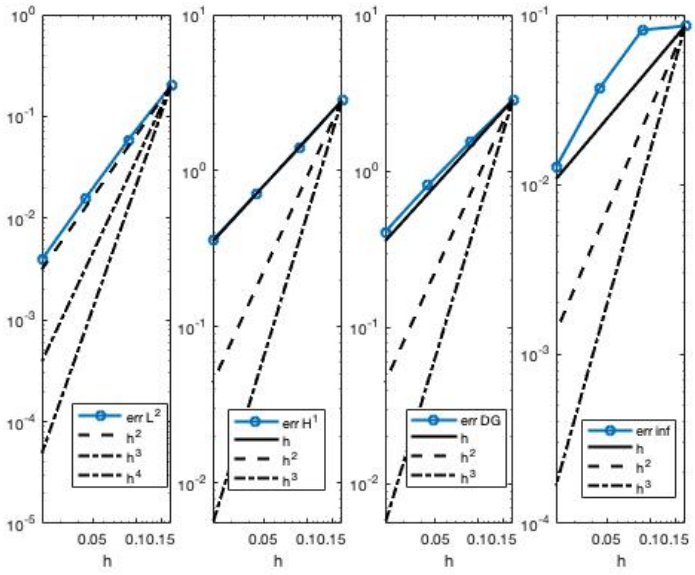

Figure 6: Convergence test of V_m

Plot of ϕ_i - intracellular potential:

Error type	**Value**
Error L^2	0.0587
Error semi-H^1	1.3895
Error H^1	1.3907
Error inf	0.0811
Error DG	1.5418

Table 2: Errors of solution Φ_i of ***Test 1***

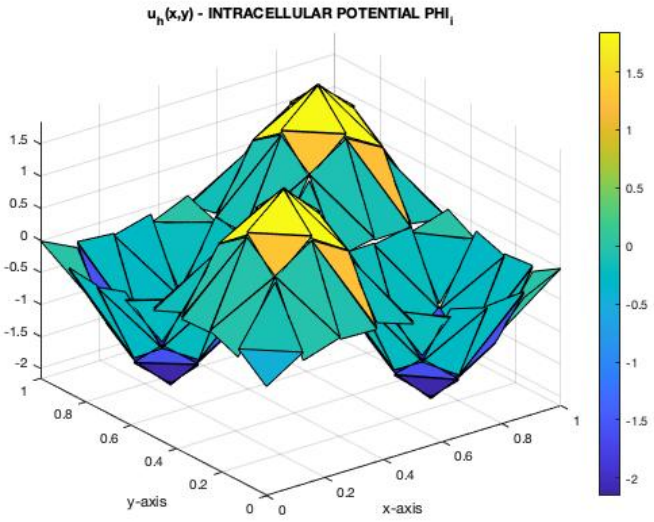

Figure 7: Numerical solution of ϕ_i

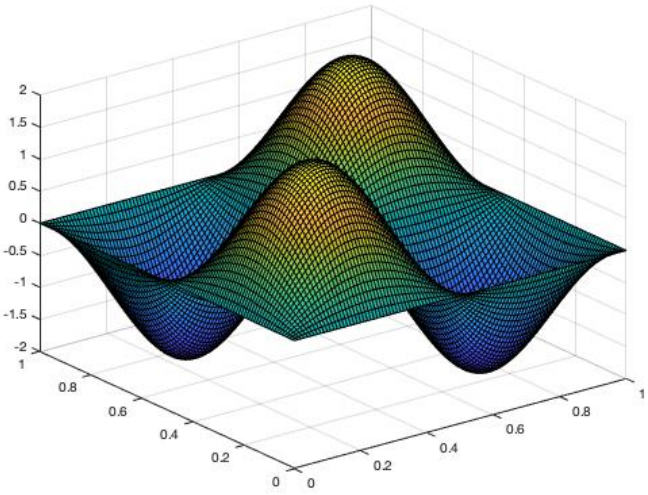

Figure 8: Analytical solution of ϕ_i

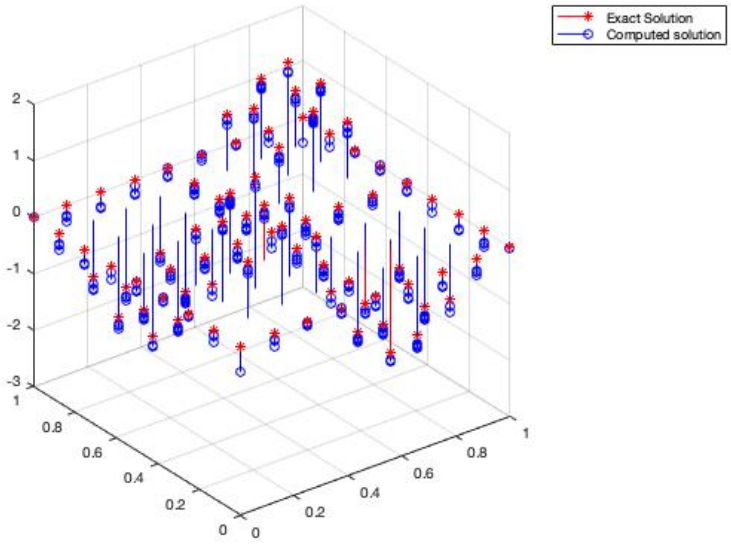

Figure 9: Error of ϕ_i

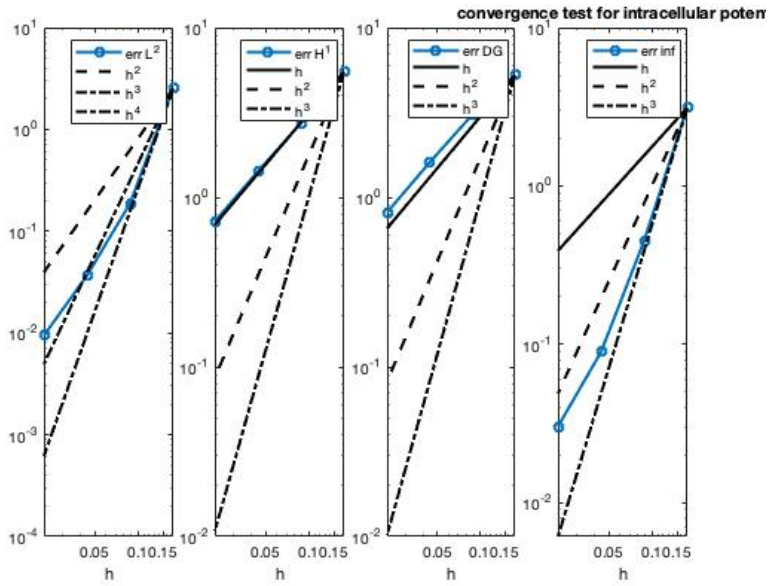

Figure 10: Convergence test of ϕ_i

Plot of ϕ_e - extracellular potential:

Error type	**Value**
Error L^2	0.1646
Error semi-H^1	1.3665
Error H^1	1.3764
Error inf	0.3693
Error DG	1.5467

Table 3: Errors of solution Φ_e of ***Test 1***

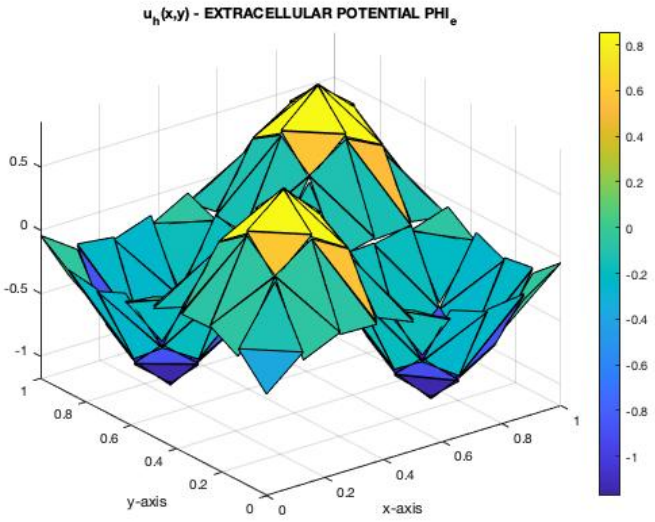

Figure 11: Numerical solution of ϕ_e

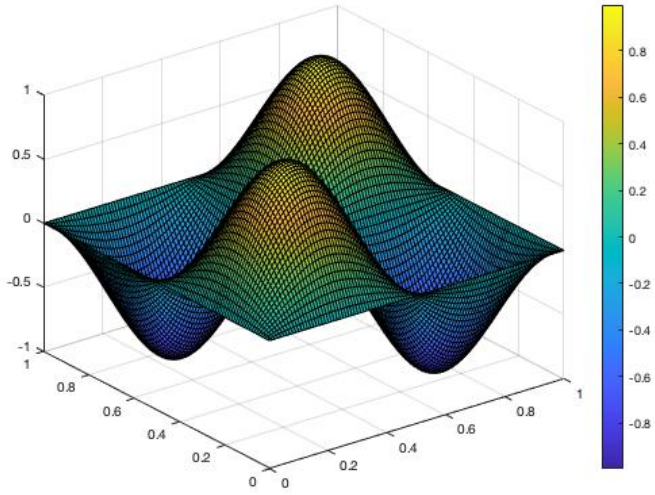

Figure 12: Analytical solution of ϕ_e

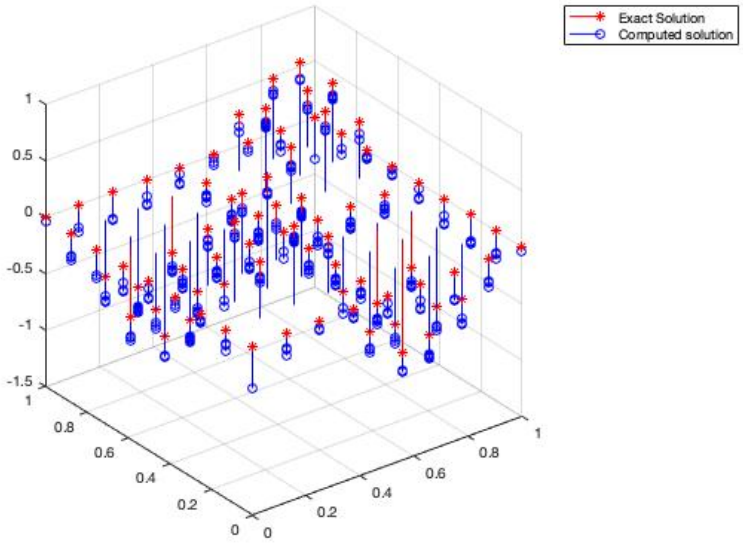

Figure 13: Error of ϕ_e

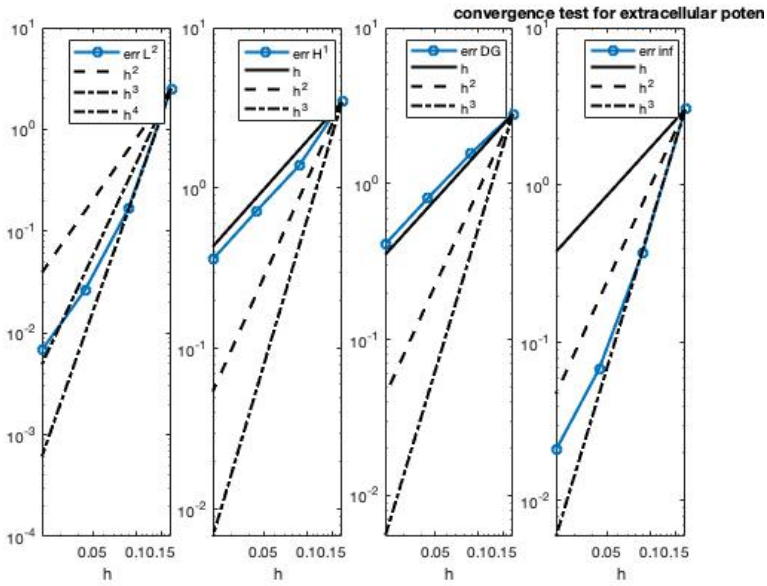

Figure 14: Convergence test of ϕ_e

6.2 *Test case 2*

Test2: k = P2, nRef = 3, $T = 0.001$, $\Delta t = 0.0001$

Error type	**Value**
Error L^2	0.0035
Error semi-H^1	0.2280
Error H^1	0.2280
Error inf	0.0076
Error DG	0.2444

Table 4: Errors of solution V_m of ***Test 2***

Plot of V_m - transmembrane potential:

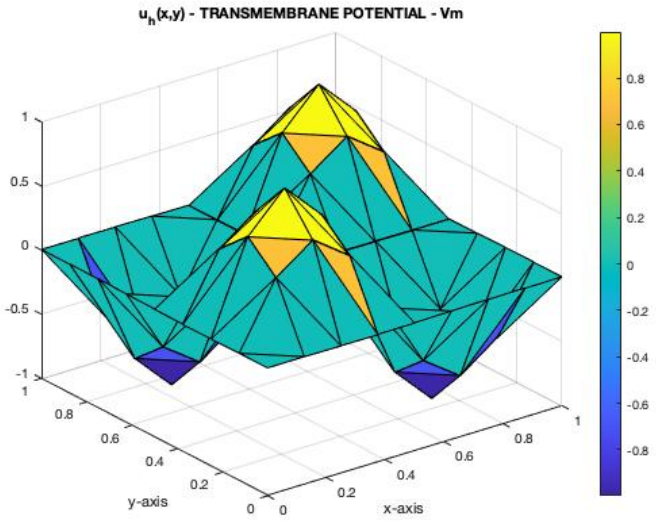

Figure 15: Numerical solution of V_m

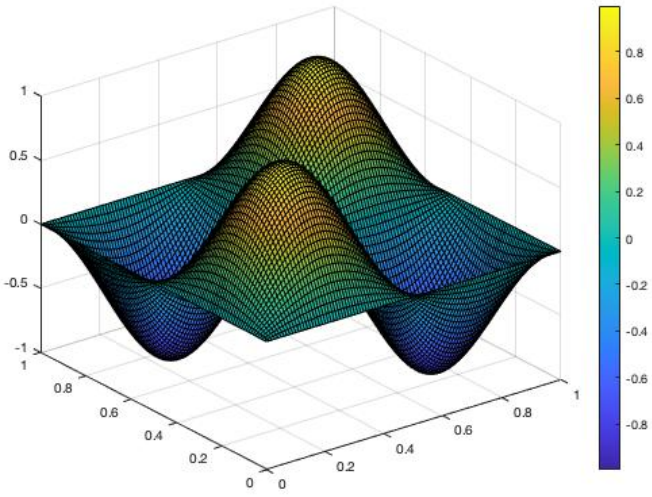

Figure 16: Analytical solution of V_m

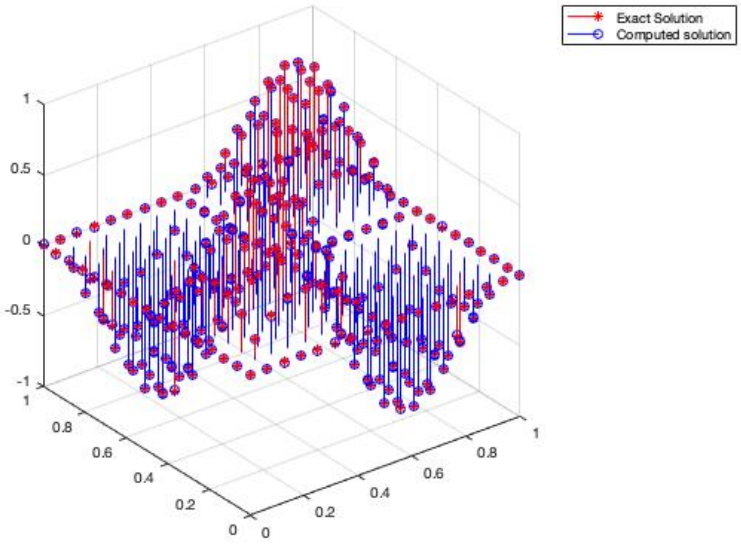

Figure 17: Error of V_m

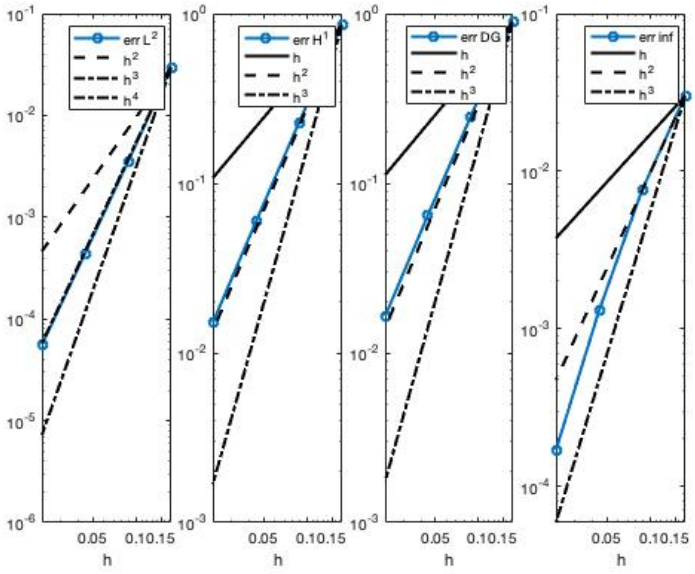

Figure 18: Convergence test of V_m

Plot of ϕ_i - intracellular potential:

Error type	**Value**
Error L^2	0.3614
Error semi-H^1	0.0490
Error H^1	0.3647
Error inf	0.3635
Error DG	0.0506

Table 5: Errors of solution Φ_i of ***Test 2***

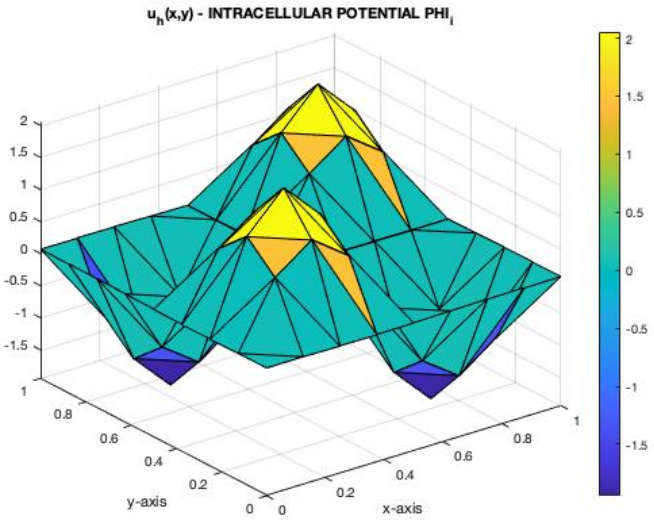

Figure 19: Numerical solution of ϕ_i

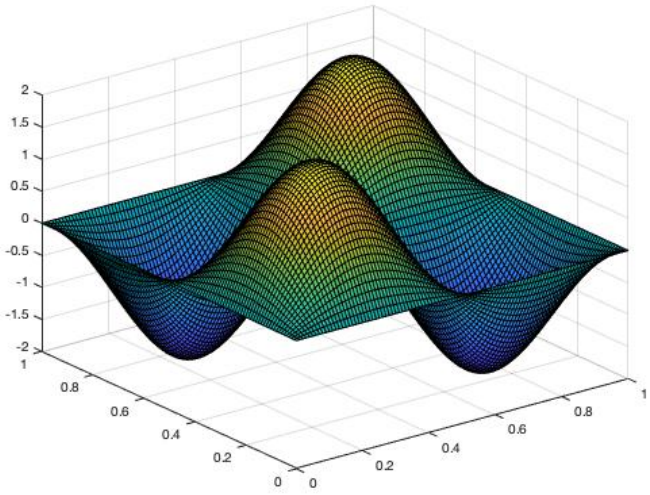

Figure 20: Analytical solution of ϕ_i

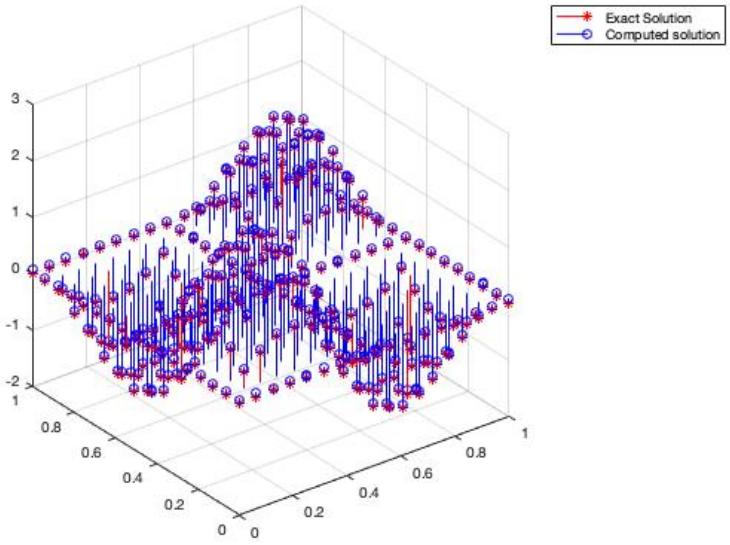

Figure 21: Error of ϕ_i

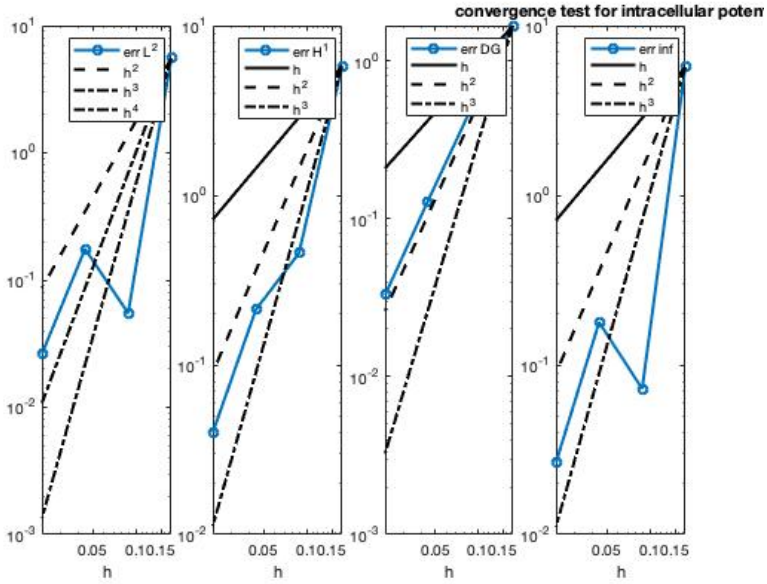

Figure 22: Convergence test of ϕ_i

Plot of ϕ_e - extracellular potential:

Error type	**Value**
Error L^2	0.3614
Error semi-H^1	0.0245
Error H^1	0.3622
Error inf	0.3624
Error DG	0.0253

Table 6: Errors of solution Φ_e of ***Test 2***

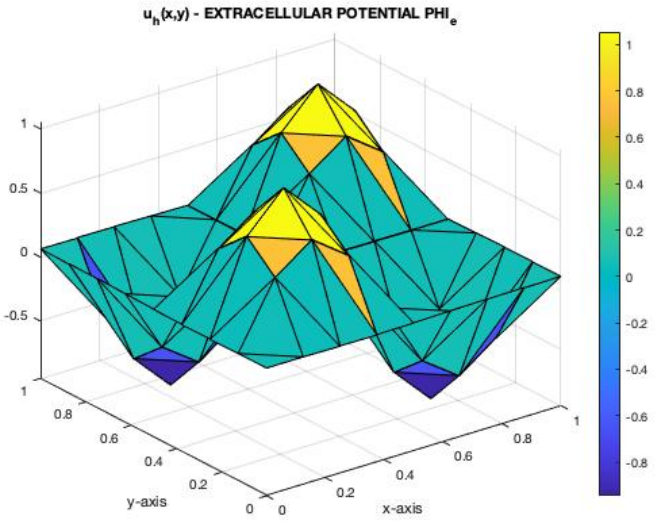

Figure 23: Numerical solution of ϕ_e

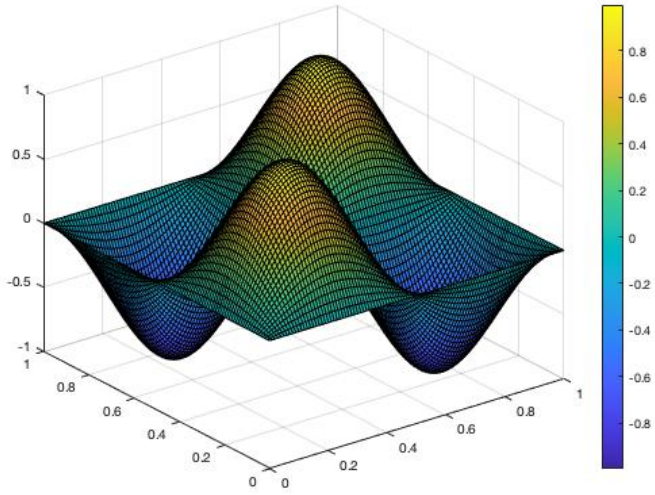

Figure 24: Analytical solution of ϕ_e

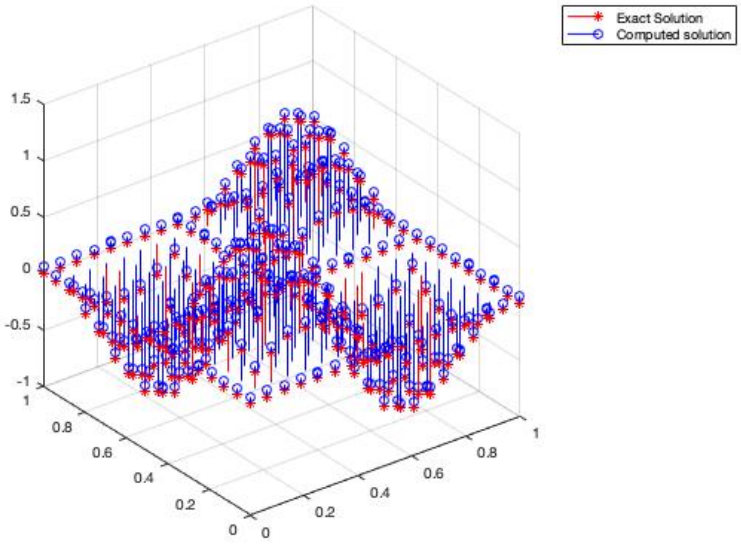

Figure 25: Error of ϕ_e

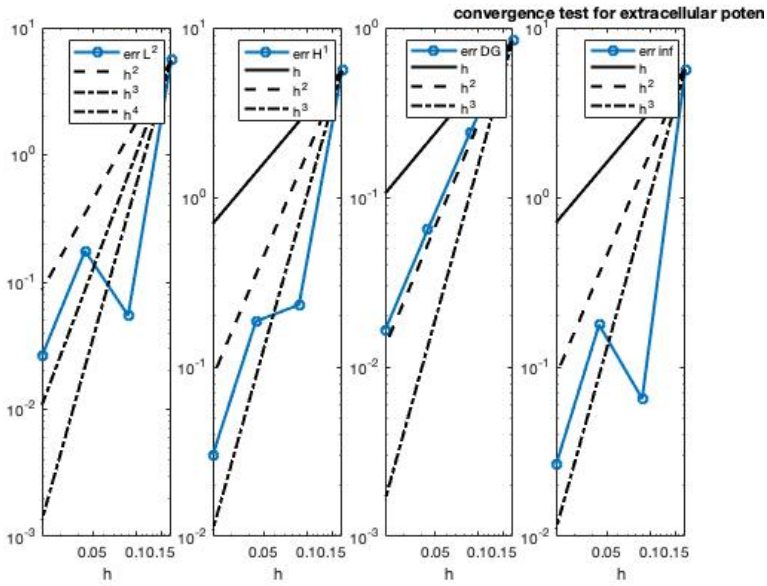

Figure 26: Convergence test of ϕ_e

6.3 *Test case 3*

Test3: k = P3, nRef = 3, $T = 0.001$, $\Delta t = 0.0001$

Error type	**Value**
Error L^2	2.7682e-04
Error semi-H^1	0.0246
Error H^1	0.0246
Error inf	0.0011
Error DG	0.0254

Table 7: Errors of solution V_m of ***Test 3***

Plot of V_m - transmembrane potential:

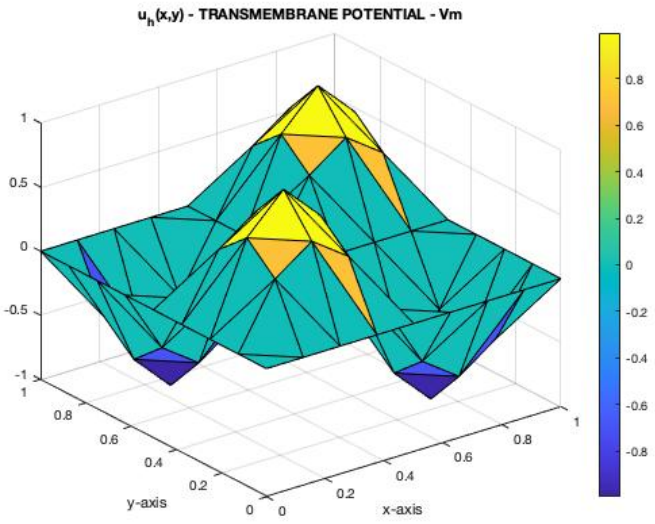

Figure 27: Numerical solution of V_m

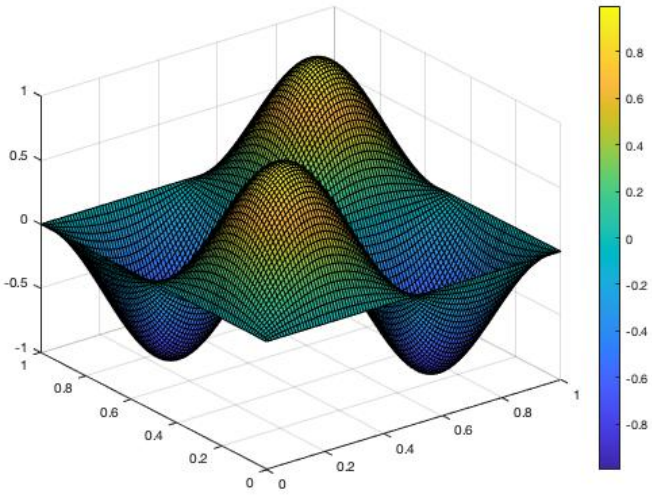

Figure 28: Analytical solution of V_m

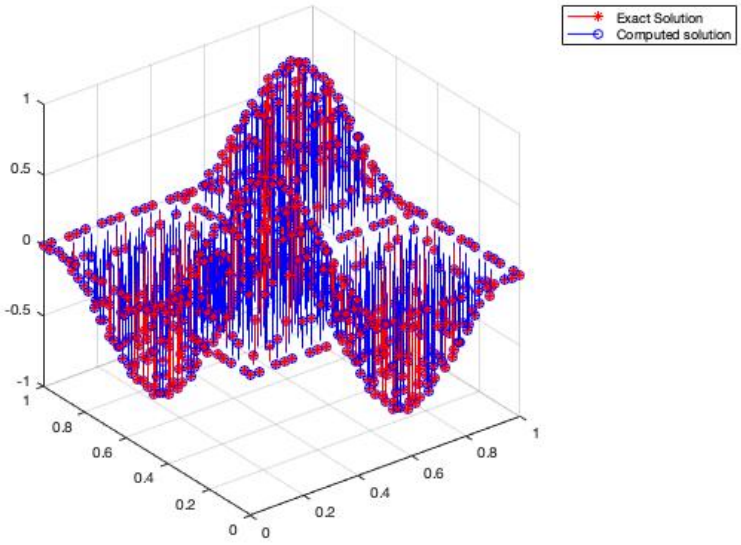

Figure 29: Error of V_m

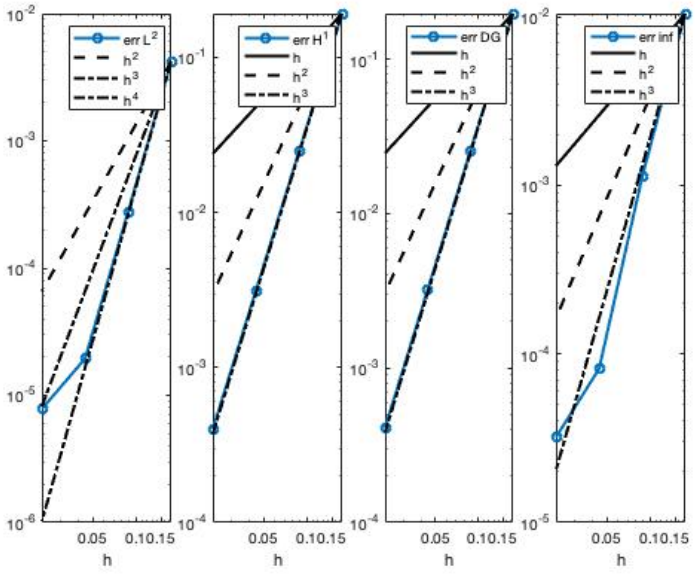

Figure 30: Convergence test of V_m

Plot of ϕ_i - intracellular potential:

Error type	**Value**
Error L^2	0.1113
Error semi-H^1	0.0490
Error H^1	0.1216
Error inf	0.1131
Error DG	0.0506

Table 8: Errors of solution Φ_i of ***Test 3***

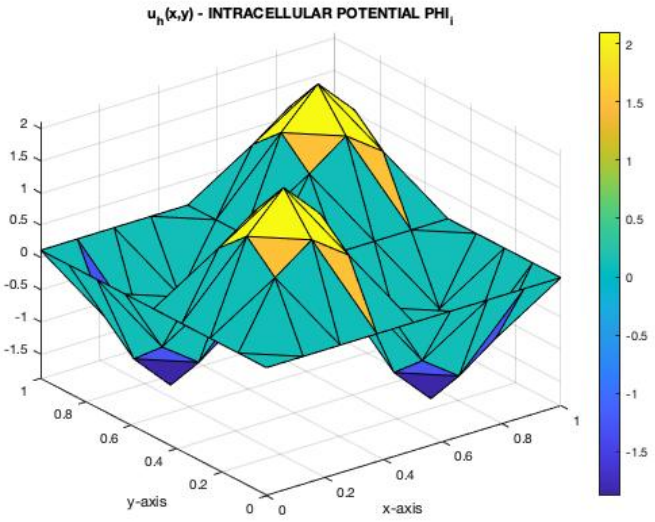

Figure 31: Numerical solution of ϕ_i

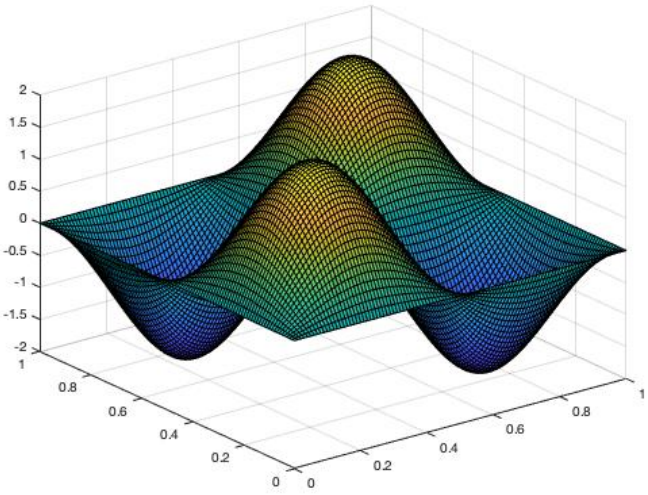

Figure 32: Analytical solution of ϕ_i

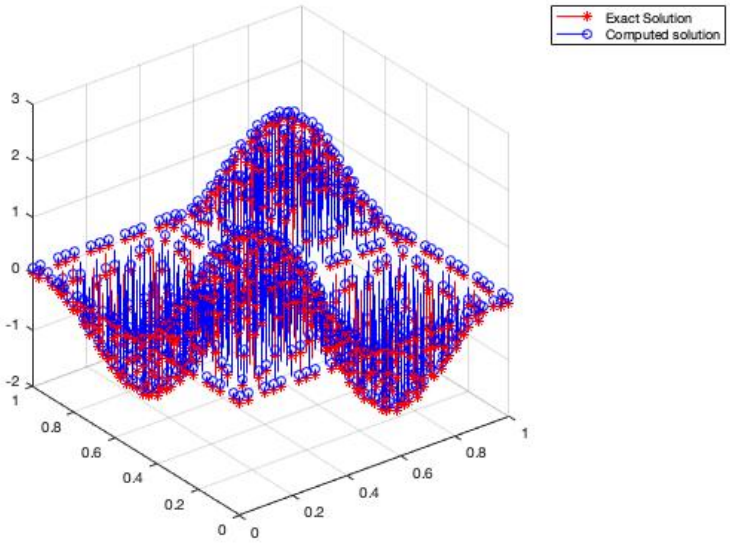

Figure 33: Error of ϕ_i

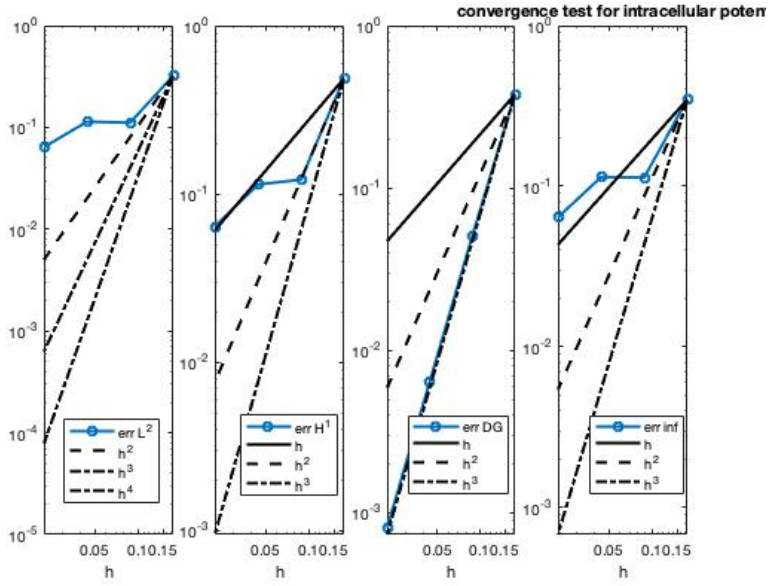

Figure 34: Convergence test of ϕ_i

Plot of ϕ_e - extracellular potential:

Error type	**Value**
Error L^2	0.1113
Error semi-H^1	0.0245
Error H^1	0.1140
Error inf	0.1123
Error DG	0.0253

Table 9: Errors of solution Φ_e of ***Test 3***

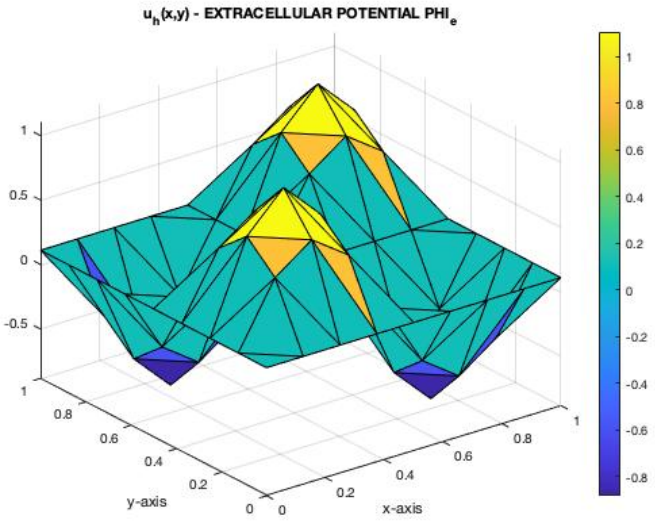

Figure 35: Numerical solution of ϕ_e

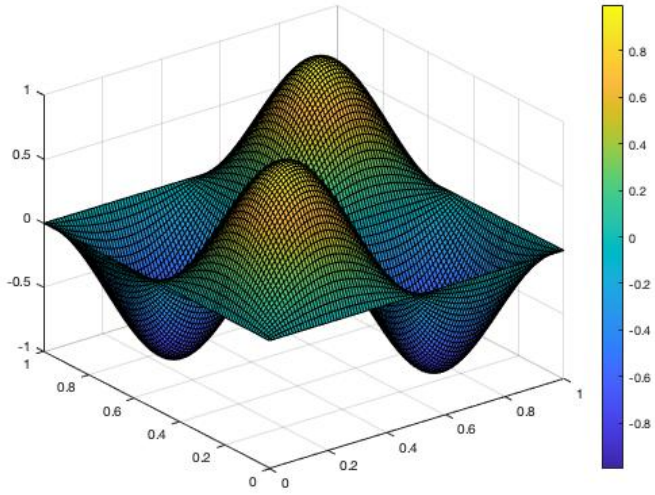

Figure 36: Analytical solution of ϕ_e

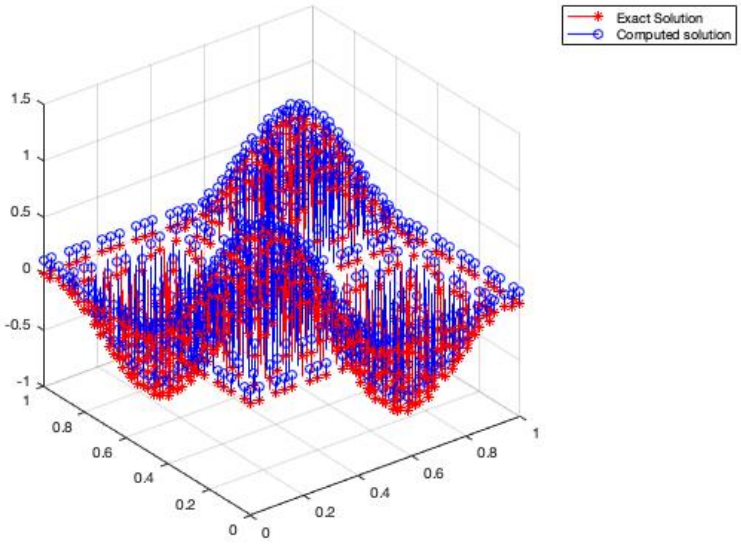

Figure 37: Error of ϕ_e

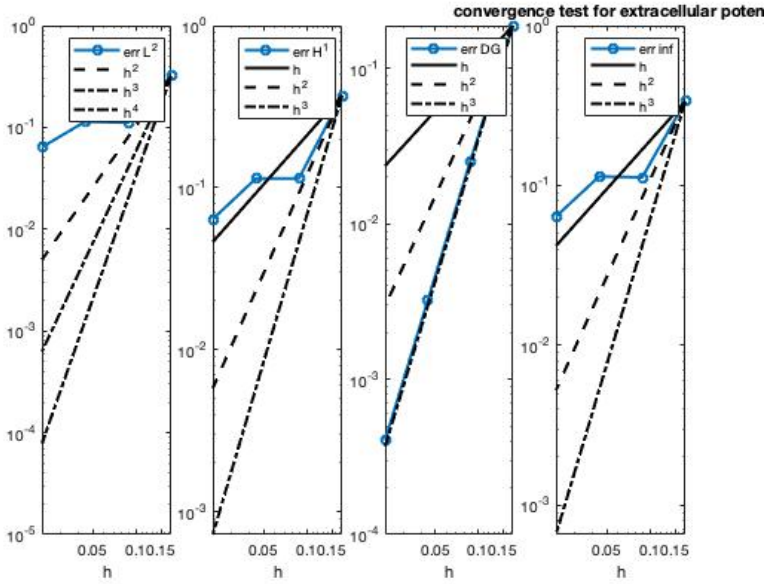

Figure 38: Convergence test of ϕ_e

6.4 *Test case 4*

Test4: k = P1, nRef = 4, $T = 0.001$, $\Delta t = 0.0001$

Error type	**Value**
Error L^2	0.0155
Error semi-H^1	0.7101
Error H^1	0.7103
Error inf	0.0365
Error DG	0.8060

Table 10: Errors of solution V_m of ***Test 4***

Plot of V_m - transmembrane potential:

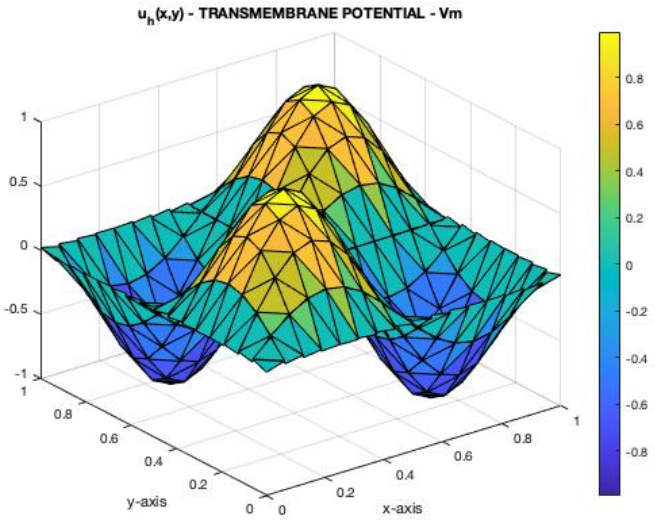

Figure 39: Numerical solution of V_m

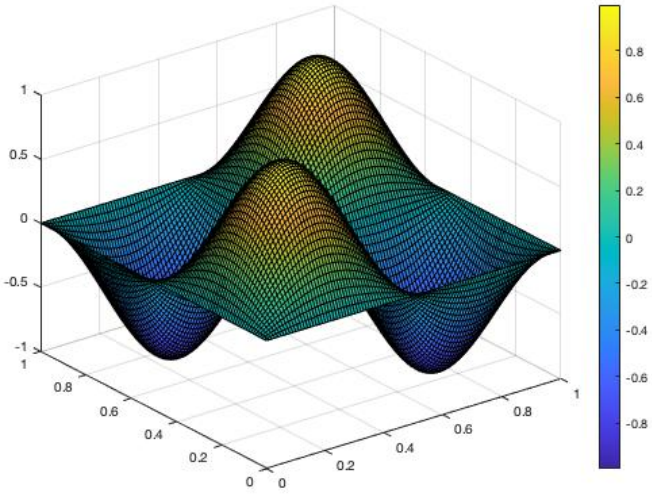

Figure 40: Analytical solution of V_m

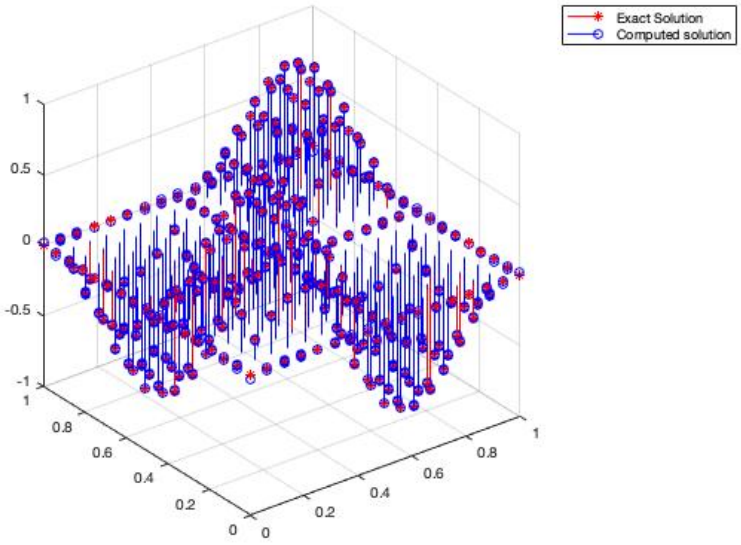

Figure 41: Error of V_m

Plot of ϕ_i - intracellular potential:

Error type	**Value**
Error L^2	0.0367
Error semi-H^1	1.4196
Error H^1	1.4201
Error inf	0.0894
Error DG	1.6071

Table 11: Errors of solution Φ_i of ***Test 4***

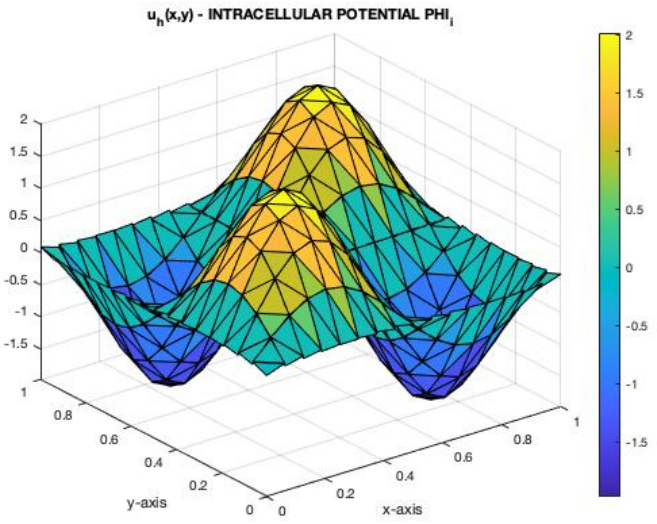

Figure 42: Numerical solution of ϕ_i

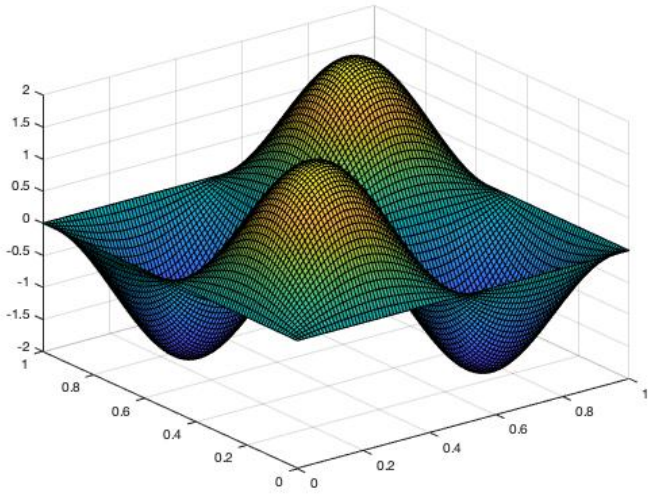

Figure 43: Analytical solution of ϕ_i

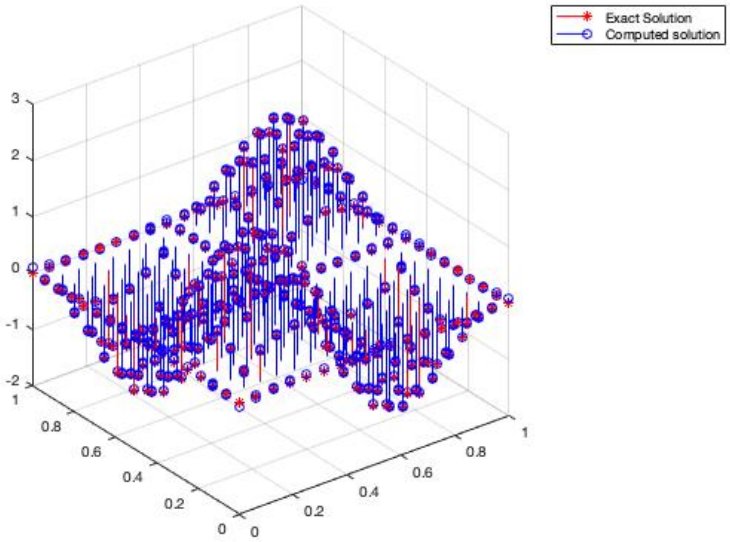

Figure 44: Error of ϕ_i

Plot of ϕ_e - extracellular potential:

Error type	**Value**
Error L^2	0.0264
Error semi-H^1	0.7125
Error H^1	0.7130
Error inf	0.0684
Error DG	0.8039

Table 12: Errors of solution Φ_e of ***Test 4***

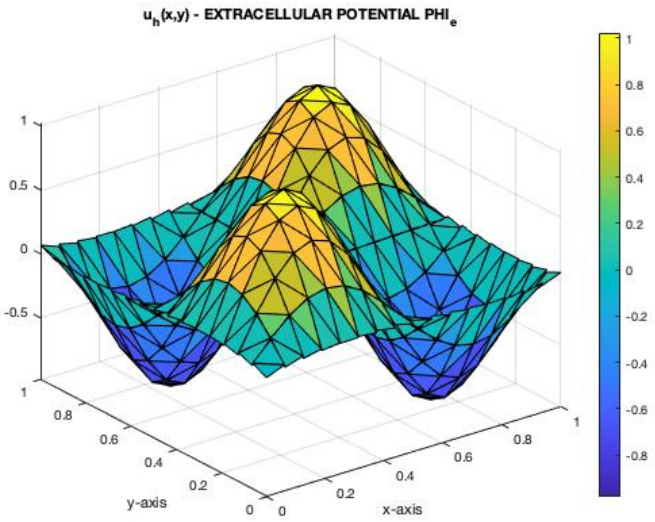

Figure 45: Numerical solution of ϕ_e

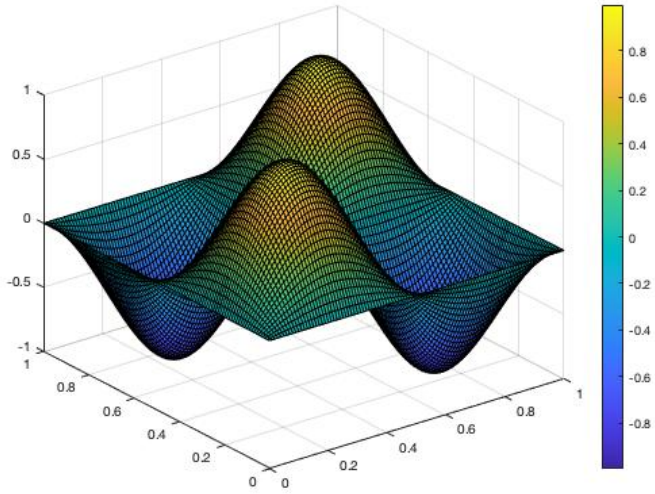

Figure 46: Analytical solution of ϕ_e

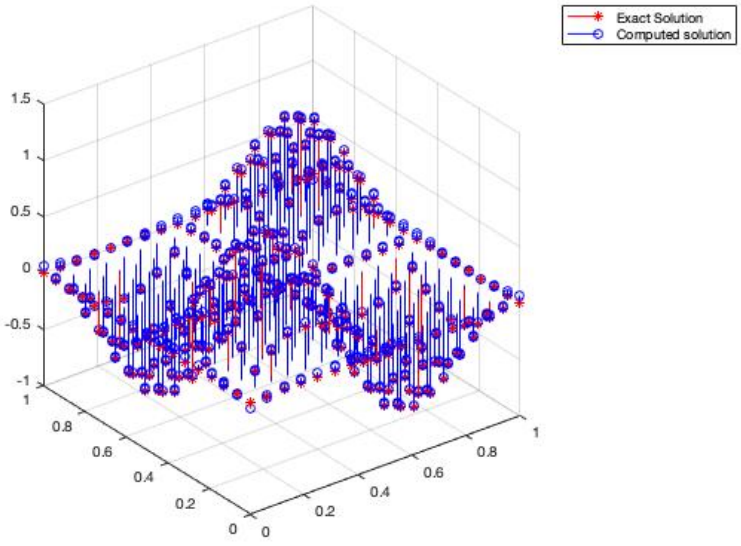

Figure 47: Error of ϕ_e

7 Convergence test of gating variable

We now investigate the convergence of the solution of the gating variable.
This need arise from the fact that the results for the intracellular and extracellular potentials are not as good as we hoped and we want to understand the behaviour of that. Just to make sure we check that the resolution of the ODE of the gating variable is correct.
As we can see from the results we reach convergence in L^2, semi-H^1, H^1, DG norms, while we don't for inf norm, as we obtained for the transmembrane potential.

Test 5.a: k = P1, nRef = 3, $T = 0.001$, $\Delta t = 0.0001$

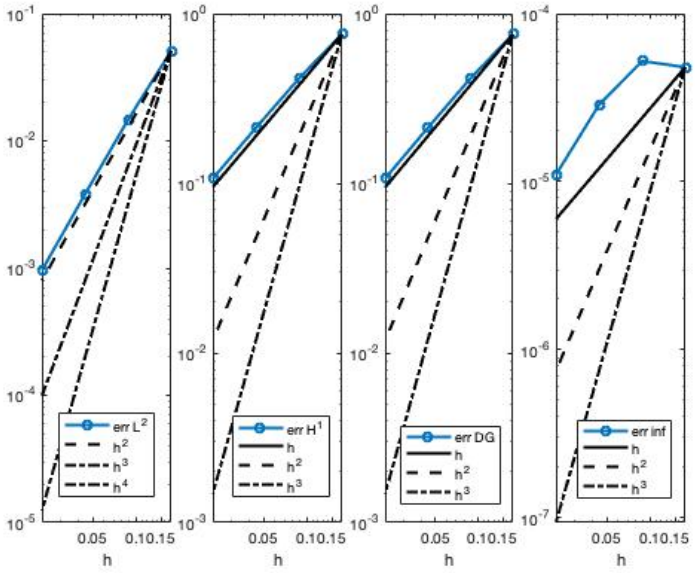

Figure 48: Error of w

Test 5.b: k = P2, nRef = 3, $T = 0.001$, $\Delta t = 0.0001$

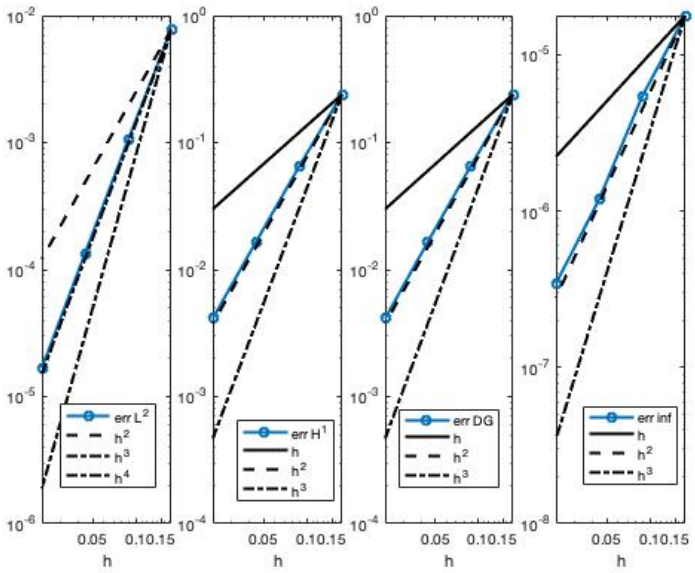

Figure 49: Error of w

Test 5.c: k = P3, nRef = 3, $T = 0.001$, $\Delta t = 0.0001$

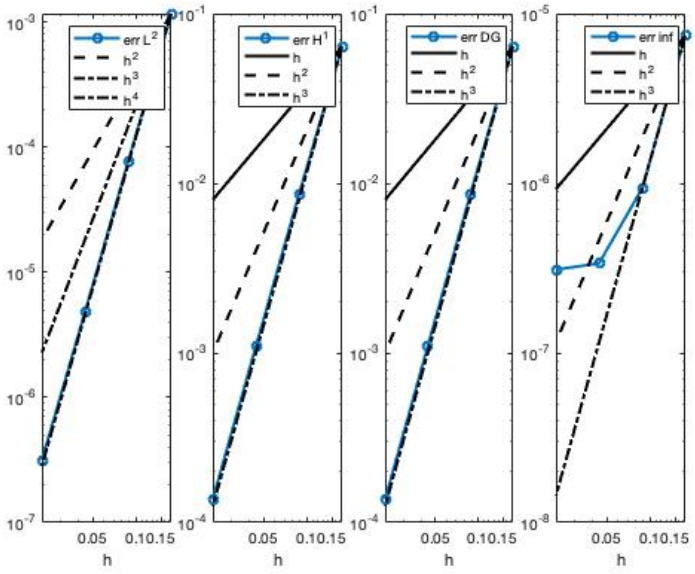

Figure 50: Error of w

8 Discussion

The implemented code reproduces a good qualitative solution as we can observe from the comparison of the numerical and analytical solutions of *Section 6*. As we can see from the error tables and plots (Figure 5, 9, 13, 17, 21, 25, 29, 33, 37, 41, 44, 47), the solution of the trasmembrane potential V_m is better then the ones of the intracellular and extracellular potentials by a quantitative point of view. This is confirmed by the fact that we reach convergence for V_m while the results seem less accurate for ϕ_i and ϕ_e.
In particular V_m converges in all of these norms (L^2, semi-H^1, H^1, DG), while it doesn't only in inf norm (see Figure 6, 18, 30).
As we can see from the error plots the boundary is where we can find the highest discrepancies between the analytical and the numerical solution. This is consistent with the fact that the boundary condition are imposed in weak form.
As expected, the errors get lower increasing the polynomial degree and the refinement of the grid.

We have also tried to run convergence test using smaller temporal steps (see Figure 51, 52, 53 - *Test 6*) and unitary parameter for the FitzHugh-Nagumo model [7] (see Figure 54, 55, 56 - *Test 7*). The first attempt was in order to verify if the observed results could be due to a temporal instability, while the second one was made to test the sensitivity of the parameter and their influences on the result.

Moreover we made a convergence test for the gating variable w of the ODE (see *Section 7*). As we can see by the reported plot we reach convergence for L^2, semi-H^1, H^1 and DG norm, but a suboptimal behaviour for the inf norm (as for the transmembrane potential).

We believe that this could be a good starting point for future projects aiming at improving our results.

***Test6* - for small temporal parameters**: $k = P3, T = 0.00001, \Delta t = 0.000001$

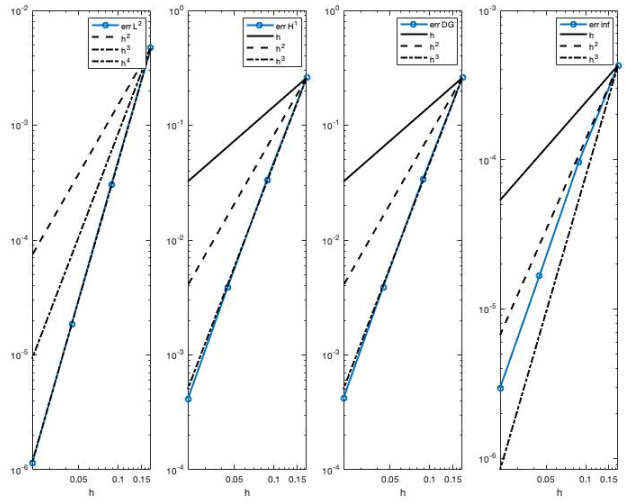

Figure 51: Convergence test for V_m with small temporal parameters

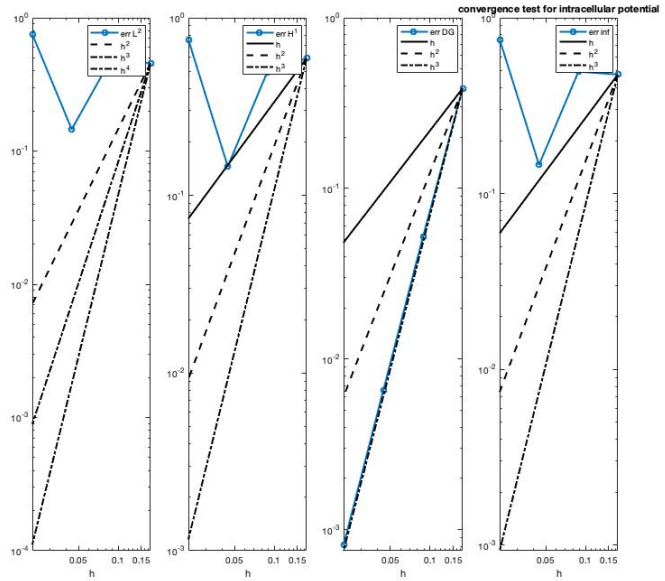

Figure 52: Convergence test for Φ_i with small temporal parameters

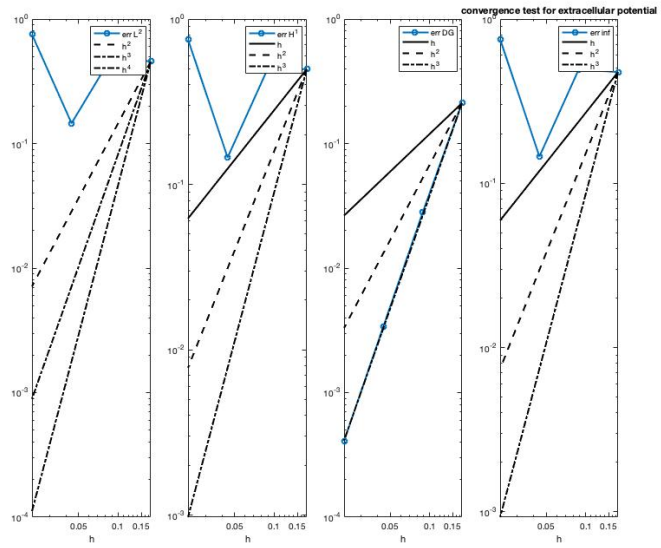

Figure 53: Convergence test for Φ_e with small temporal parameters

***Test7* - unitary parameter for the FitzHugh-Nagumo model**: $k = P3, T = 0.001, \Delta t = 0.0001$

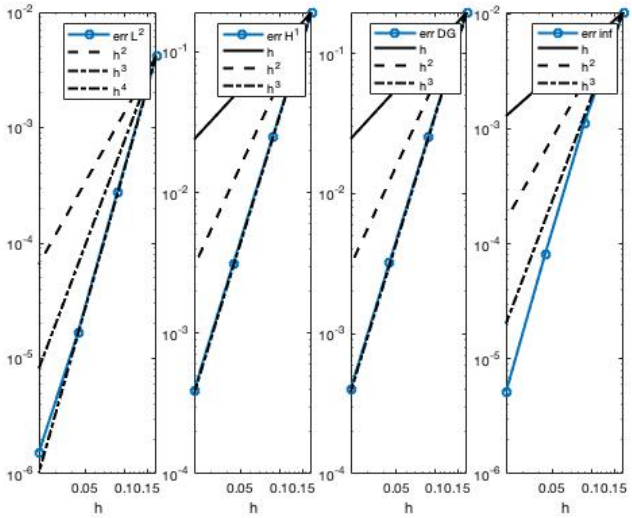

Figure 54: Convergence test for V_m with unitary parameters

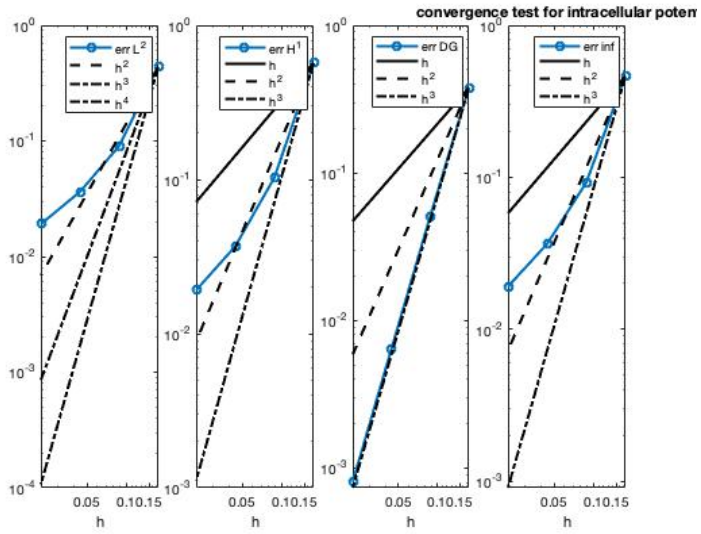

Figure 55: Convergence test for Φ_i with unitary parameters

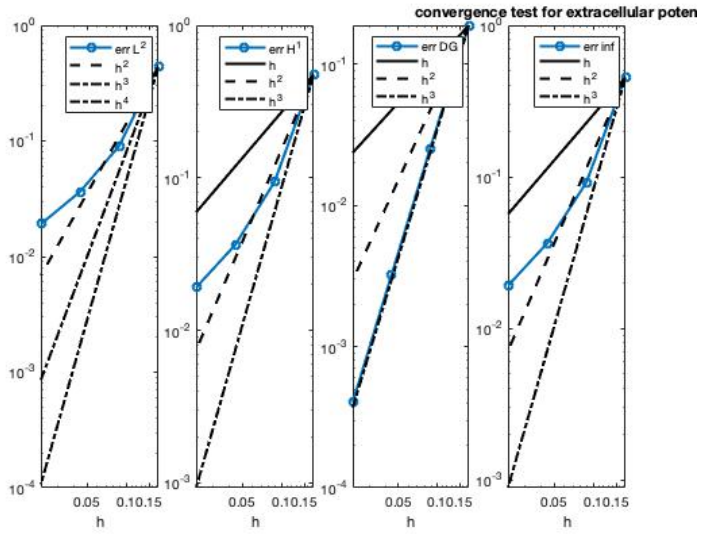

Figure 56: Convergence test for Φ_e with unitary parameters

9 Code implementation

The main difference with the previous code lies in the passage from the monodomain to the bidomain. It involves the resolution of a block matricial system and not of a unique equation as in the former implementations.
Here we report the temporal loop of the resolution of the block system where we solve it with the backslash command:

```
for t=dt:dt:T

    Vm0 = u0(1:ll) - u0(ll+1:end);
    w1 = 1/(1+epsilon*gamma*dt)*(w0+epsilon*dt*Vm0);
    w1=cat(1,w1, w1);

    fi = assemble_rhs_i(femregion,neighbour,Data,t);
    fe = assemble_rhs_e(femregion,neighbour,Data,t);
    f1 = cat(1, fi, fe);

    [C] = assemble_nonlinear(femregion,Data,Vm0);
    NONLIN = [C -C; -C C];


    r = f1 + ChiM*Cm/dt * MASS * u0 + ChiM * MASS_W *w1;

    u1 = ( ChiM*Cm/dt * MASS + (STIFFNESS + NONLIN)) \ r;


    f0 = f1;
    u0 = u1;
    w0 = w1(1:ll);
end
```

Starting from the definition of the stiffness matrices, we needed to introduce different implementation for the intra and extracellular solutions (and not only different input variables for the same script) due to the different conductivities Σ_i and Σ_e.

Moreover, also the implementation of convergence tests, compute errors, post processing and assemble rhs functions needed to be made specific for the three different solutions, V_m, ϕ_i and ϕ_e.

This code has been implemented for our test with Neumann boundary condition: in the script "matrix2D.m" the boundary terms implemented are the ones derived from the integration of the diffusive part.

Finally we also implemented a convergence test for the gating variable ω, used to check the accuracy of this solution.

References

[1] A. Quarteroni, A. Manzoni and C. Vergara. *"The cardiovascular system: Mathematical modelling, numerical algorithms and clinical applications"*. Cambridge University Press, 2017.

[2] Francesco Andreotti and Davide Uboldi. *"Discontinuouns Galerkin methods applied to Monodomain problem"*. 2021.

[3] Note of the course of *"Numerical Analysis of Partial Differential Equation A.Y. 2018-2019"* of Professor Paola Francesca Antonietti.

[4] Clara Pigolotti. *"A discontinuous Galerkin approach for cardiac electrophysiology"* 2018/2019.

[5] James Keener, James Sneyd, James Keener, James Sneyd. *"Mathematical Physiology I Cellular Physiology"*. Springer-Verlag New York, 2009.

[6] Arnold, Brezzi, Cockburn, Marini. *"Unified Analysis of Discontinuous Galerkin Methods for Elliptic Problems"*. SIAM Journal on Numerical Analysis, 2004.

[7] FitzHugh. *"Impulses and physiological states in theoretical models of nerve membrane"*. Biophys. J. 1, 445–466. 1961.

[8] G. Beeler and H. Reuter. " Reconstruction of the action potential of ventricu- lar myocardial fibres". J. Physiol. 268, 177–210. 1977.

[9] Luo and Y. Rudy *"A dynamic model of the cardiac ventricular action potential, I: Simulations of ionic currents and concentration changes"* and *" A dynamic model of the cardiac ventricular action potential, II: Afterdepolarizations, triggered activity, and potentiation"*. Circ. Res. 74, 1071–1096. Circ. Res. 74, 1097–1113. 1994.

[10] Niederer SA, Kerfoot E, Benson AP, Bernabeu MO, Bernus O, et al. " Verification of cardiac tissue electrophysiology simulators using an N-version benchmark." Philosophical Transactions of the Royal Society A: Mathematical, Physical and Engineering Sciences 369: 4331–4351. 2011.

[11] Hüsnü Dal , Serdar Göktepe , Michael Kaliske Ellen Kuhl. *"A fully implicit finite element method for bidomain models of cardiac electrophysiology "*. Computer Methods in Biomechanics and Biomedical Engineering (pg 645-656). 2011.

[12] Serdar Göktepe Ellen Kuhl. *"Computational modeling of cardiac electrophysiology: A novel finite element approach"* International Journal for Numerical Methods in Engineering. 2009.

[13] McKean. *"The McKean's Caricature of the Fitzhugh–Nagumo Model I"* SIAM Journal on Numerical Analysis. 1970.

[14] John Rinzel. *"Nonlinear Phenomena in Physics and Biology - Models in Neurobiology"*

[15] M. F. Wheeler. "An elliptic collocation-finite element method with interior penalties." SIAM J. Numer. Anal., 15(1):152–161, 1978.

[16] B. Rivi'ere, M. F. Wheeler, and V. Girault. "Improved energy estimates for interior penalty, constrained and discontinuous Galerkin methods for elliptic problems." Comput. Geosci., 3(3-4):337–360 (2000), 1999.

[17] J. Rogers and A. McCulloch. "A collocation-Galerkin finite element model of cardiac action potential propagation", IEEE Trans. Biomed. Engrg 41, 743–757. 1994.

[18] Bueno-Orovio, E. Cherry and F. Fenton . "Minimal model for human ventricular action potentials in tissue", J. Theoret. Biol. 3, 544–560. 2008.